# THE EFFECTS OF DEPOSITION CONDITIONS ON THE MECHANICAL PROPERTIES OF TITANIUM SILICON NITRIDE NANOCOMPOSITE COATINGS

by

SUO LIU

Presented to the Faculty of the Graduate School of

The University of Texas at Arlington in Partial Fulfillment

of the Requirement

for the Degree of

MASTER OF SCIENCE IN MATERIALS SCIENCE AND ENGINEERING

THE UNIVERSITY OF TEXAS AT ARLINGTON

MAY 2015

Acknowledgements

Foremost, I would like to express my sincere gratitude to my advisor Dr. Efstathios I. Meletis for the continuous support of my graduate study and research, for his patience, motivation, enthusiasm, and immense knowledge. His guidance helped me in all the time of research and writing of this thesis. Besides my advisor, I would like to thank the rest of my thesis committee, Dr. Fuqiang Liu and Dr. Harry F. Tibbals, for their generous help.

My sincere thanks also go to Dr. Jessica Mooney for preparation of the samples used in this study, as well as for training me on the optical profilometer.

I thank each and every one of my group members for their advice, their help and their friendship. I thank Yishu Wang for his help with XPS.

Last but not least, I would like to thank my family: my parents Dao Feng Xiang and Aiping Liu, for supporting me spiritually throughout my life.

April 28, 2015

Abstract

THE EFFECTS OF DEPOSITION CONDITIONS ON THE MECHANICAL PROPERTIES OF TITANIUM SILICON NITRIDE NANOCOMPOSITE COATINGS

Suo Liu, M.S.

The University of Texas at Arlington, 2015

Supervising Professor: Efstathios I. Meletis

Titanium Silicon Nitride has received much attention in recent years for its theoretical super hardness and oxidation resistance at high temperature. In this work, the mechanical properties of TiSiN thin films including hardness, coefficient of friction, wear rate, wear mechanism were studied in detail using nanoindentation, pin-on-disk tribometer, optical profilometer, scanning electron microscope (SEM) and X-ray photoelectron spectroscopy (XPS). Four deposition conditions were varied to find the optimal conditions that produce the TiSiN film with the highest hardness and the best wear resistance. First, four substrate biases

(100 V, 200 V, 300 V, and 500 V) were used, respectively. Then, different power (50 W, 55 W, 60 W) and different $N_2$ ratio (20%, 25%) were applied to Si target. Finally, three rotation speeds of the substrate holder (1 RPM, 3 RPM, and 6 RPM) were utilized.

The study results demonstrated that TiSiN coating deposited at 100V bias, 60 W Si power, 25%$N_2$ gas mixture, and 6 RPM rotation speed has the highest hardness of 38.9 GPa. High COFs of greater than 1.0 were observed in all films tested. Wear rates increased as the hardness of the film decreased. The wear mechanism was attributed to be a three body wear due to the presence of counter material debris in the wear track.

Table of Contents

List of Figures

List of Tables

# Chapter 1

# INTRODUCTION

## 1.1 Introduction and Motivation

Diamond is the hardest material known to man, with a hardness of from 70 GPa up to 100 Gpa. It is extremely hard due to its high coordination number and strong nonpolar covalent carbon to carbon bonding. These types of hard materials are referred as intrinsically hard materials. Other examples of intrinsically hard materials may include cubic boron carbide, with hardness in the range of 46 GPa to 48 GPa [1, 2]. However, these intrinsically hard materials are expensive and difficult to process for desired application such as hardware protective coatings. Therefore, in an attempt to synthesize new materials that possess hardness comparable to diamond and can be used in coating application, extrinsically hard materials have gained much attention in recent years. The hardness of extrinsically hard materials, unlike that of intrinsically hard materials, is a result of nanostructure within the material, which would act as a barrier for plastic deformation [1].

Traditional coating applied to machine tools is mainly TiN, with hardness of around 24 GPa. It can withstand oxidation up to 400 $^{\circ}$C [3]. One new system developed in recent years is TiSiN, with theoretical modeling suggested hardness of 100 GPa. Early research showed that addition of silicon into traditional

tribological coating material TiN resulted in hardness of 70 GPa [4]. Veprek in his work along with others suggested this high hardness is a result of quasi-binary phase system consisted of nanocrystalline TiN grain and monolayer of amorphous $Si_3N_4$, which act as a barrier for dislocation movement at grain boundaries [4, 5]. Researchers also found that TiN grain size reduction by adding Si contributes to its high hardness as well. Si addition to TiN may also increase the oxidation resistance from 400 $^{\circ}$C to 600 $^{\circ}$C [3].

There are many different synthesis methods used to produce TiSiN thin film, such as plasma chemical vapor deposition (PCVD), arc plasma deposition, laser ablation, physical vapor deposition, etc. This variation in synthesis method and condition result in a variety of stoichiometry and properties.

This study will focus on effect of physical wear behaviors of TiSiN thin film deposited with different parameters.

## 1.2 Objective

Theoretical calculations and researches demonstrated that TiSiN has the potential to be a new super hard material that may be suitable for coating application.

The aim of this study is:

To determine the effect of deposition parameters such as substrate bias, silicon power, $N_2$ to Ar ratio and rotation speed of target on the mechanical

properties of TiSiN thin film coating.

# Chapter 2

# LITERATURE REVIEW

In the past few decades, technology is advancing with each passing day. To meet the needs of technological advancement, research for new materials received much attention. In coating application for tools, weaponries, and technology, TiSiN showed promising mechanical properties. Theoretical calculation suggested TiSiN can be as hard as diamond, and has good oxidation resistance around 600 ˚C -800 ˚C [1, 2, 6-10]. These properties enabled a great potential for TiSiN in coating applications that require high hardness.

## 2.1 Intrinsically Hard Material

Hard materials, in large, can be divided into two categories: intrinsically hard material and extrinsically hard materials. Intrinsically hard materials are hard due to its high coordination number and strong covalent bonding. Diamond is the hardest material known to men for a long time. It has a high coordination number of 4 and strong non-polar carbon-carbon covalent bond. It is a perfect example for intrinsically hard materials with hardness from 70 GPa to 100 GPa [1, 9]. Another well know intrinsically hard material is cubic boron nitride, which has hardness greater than 40 GPa [1]. However, intrinsically hard materials are limited in technological applications such as machinery coating. Taking diamond for

example, it has great mechanical hardness but cannot withstand high temperature above 800 ˚C. Diamond is also too expensive and difficult to machine.

### *2.1.1 Recent Attempts to Design New Intrinsically Hard Material*

Recent attempt to synthesize new intrinsically hard material began about three decades ago by Marvin L. Cohen, a professor from UC Berkley. In his calculation, he suggested carbon nitride, $C_3N_4$, a new intrinsically hard material, which would attain hardness between cubic boron nitride and diamond. Unfortunately, this theory was later denied by experimental results which showed its hardness is below 30 GPa [12]. Other attempts include Osmium Boride ($OsB_2$) [13], Rhenium Diboride ($ReB_2$) [14, 15], Boron Suboxide ($B_6O$), which of those failed to beat c-BC in hardness [16].

## 2.2 Extrinsically Hard Materials

To meet the technological needs, researchers turned their attention to the new engineered extrinsically hard materials. Extrinsically hard materials attain their hardness through design and control of their micro (nano) structures and grain size. There are mainly two types of mechanisms for hardness enhancement of extrinsically hard materials.

### *2.2.1 Heterostructures Enhancement*

First mechanism is acquired by heterostructures made of periodically alternating layers of two different materials, which are a few nanometers in thickness with largely different shear moduli. This idea proposed by Koehler suggested that each layer is so thin that no dislocation will operate within the layer, and due to the elastic repulsion formed between the two different layers would reject the movement of the dislocation in the less stiff layer towards interface [17]. Many different researches have been conducted to prove this theory. For example, heterostructures formed of two immiscible metals showed higher hardness in tensile test [17]. Other experiments conducted using transition metal nitride showed more than 200% of hardness enhancement [1, 6-11]. Figure 2.1 shows the relationship of multilayer period in nanometer and hardness enhancement. An increase in hardness is observed initially as the period decreases. However, in smaller scale, further decrease in period will result in a decrease in hardness. According to Barnett's research, this phenomenon is due to roughness of the interface [18, 19].

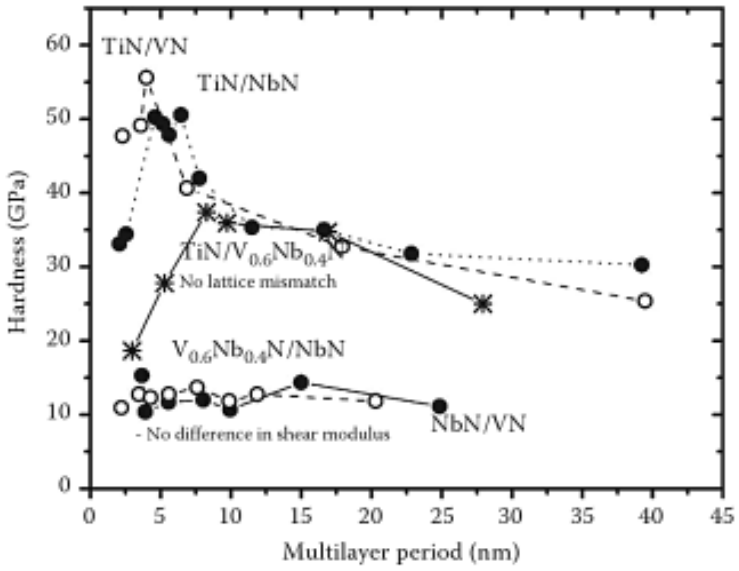


Figure 2.1. Relationship of hardness and layer periods in transition metal heterostructures [18, 19]

*2.2.2 Grain Size Enhancement*

Dislocation generation, multiplication and motion are major factors contributing to plastic deformation. Limiting or eliminating these factors can increase hardness significantly. One method of doing so is by reducing grain size of interested material. According to Hall-Petch relation, hardness of a single phase material increases as the grain size decreases in the micro and nano regime. This effect would reverse when the grain size reaches below about 10 nanometers: decreasing grain size reduces hardness, as shown in Figure 2.2 [20-22]. A material with large grain size tend to have more dislocations, which means it has more driving force for dislocation to move from one grain to another. Reducing size of

the grain can effectively decrease the number of dislocations and the ability for the dislocation to move. Nano size crystal is free of dislocation and therefore retains high hardness. When the grain size decreases below 10 nm, grain boundary increases and will subject to grain boundary sliding which reduces hardness of the material [20-22].

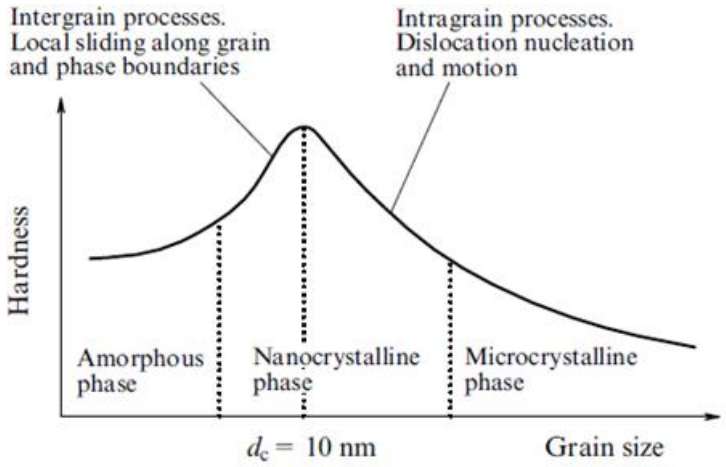


Figure 2.2. Hall-Petch Relationship between hardness and grain size

Carsley et al came up with a relationship describing the transition between the effect and the reverse effect of Hall-Petch relation in Equation 2.1 [23].

$$\mathrm{H(d)} = f * (\mathrm{H_0} + \beta * d^{-0.5}) + (1 - f) * H_{GB} \quad (2.1)$$

Where:

H(d) is the hardness of small grain size d

$H_0$ is the hardness of large size, single crystals of the material

$H_{GB}$ is the hardness of the material considered in bulk

$f$ is the volume fraction of small crystal of size d

β is the proportionality factor of the Hall-Petch strengthening

$(H_0 + \beta * d^{-0.5})$ represents the hardness enhancement with decrease grain size due to Hall-Petch strengthening.

*2.2.3 Ion Bombardment at Low Temperature*

The surface of the synthesizing film is bombarded with ions during the deposition due to the applied bias on the substrate and internal pressure. Ion bombardment may also contribute to the hardness enhancement of the deposited film. Ion bombardment with energy greater than 40 to 50 eV can create denser and smoother film [24]. This is due to the bombardment creating displacement damage in the lattice, as well as building up compressive stress in the film. However, this effect is not permanent, as the annealing would completely remove the effect and decrease hardness to its original value. For example, researchers were able to produce TiN film with hardness of 80 GPa at low temperature with reactive sputtering. The enhanced hardness decreases to its original value as the sample annealed and got rid of the effects caused by the ion bombardment [25]. See figure 2.3 for an example of the relationship of decreasing hardness and annealing.

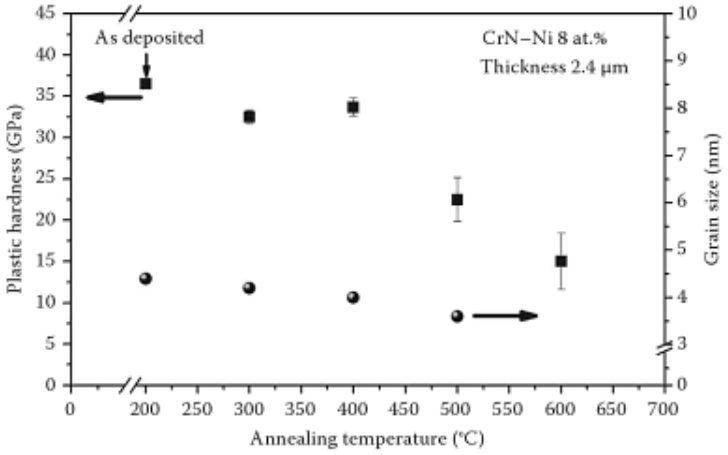


Figure 2.3. Hardness of sample prepared at low temperature vs. annealing temperature for 30min vs. grain size [25]

*2.2.4 Thermal Stability of Nanostructured Materials*

Thermally instability is a challenge faced by all fine grain materials. When compared to the coarsely grained materials, materials with finer grain tended to undergo Ostwald Ripening, which is a coarsening process of inhomogeneous structure changes overtime. During this process the smaller particles dissolve and redeposit onto larger particles that is considered to be more electronically stable. In application for thin film coating, it would most likely be used in harsh environment where high temperature is expected. Thus, coarsening due to recrystallization is a problem that needs to be solved. Veprek, in his paper, suggested two methods to avoid this problem, first, by controlling the kinetics of the nanostructure system, and second, by controlling the thermodynamics of the

system [1, 26, 27].

## 2.3 Transition Metal Silicon Nitride

Tribological coatings are normally applied on the surface of a part of tools or equipment that is subject to frequent wear and tear. Therefore, applied coating requires high hardness, high wear resistance, and depending on the requirements of the application, high oxidation resistance at elevated temperature. One of the first coatings developed was titanium carbide coatings using Chemical Vapor Deposition in 60s'. Titanium nitride was developed in 80s' using Physical Vapor Deposition, and it has since been used in various mechanical parts and tools because of its good hardness, low coefficient of friction and chemical stability. [24-34]. However, the oxidation resistance of TiN coating is not satisfactory. Although both coatings are still widely used in today's industries, scientists have started to develop new tribological coatings that will meet the needs of new technological advancements. Li et al. developed a new system by adding silicon into titanium nitride and reported hardness enhancement up to 70 GPa from 18 to 21 GPa [1, 4].

### *2.3.1 Titanium Silicon Nitride*

Titanium Silicon Nitride has received much attention for its theoretical super hardness and oxidation resistance at high temperature. Many studies have been

conducted to investigate the actual achievable hardness of TiSiN coating. Consistent hardness of 40 GPa to 50 GPa has been reported [33, 38, 39]. Another property drawing interest in TiSiN for coating application is its high oxidation resistance. Experimental results showed that it is capable of resisting oxidation up to 700 ˚C [38, 40-42]. Researchers found that by adding silicon into titanium nitride, the grain size would decrease and the formation of amorphous $Si_3N_4$ which would act as a barrier for dislocation movement.

### *2.3.2 Hardness Enhancement in TiSiN Coatings*

TiSiN coatings are not intrinsically hard materials like diamond and cubic boron carbide which have high coordination number and strong covalent bonding. It is rather a nano-composite material consisting of two phases, nc-TiN/a-$S_3N_4$ (nanocrystalline TiN and amorphous $S_3N_4$). It is believed that the super hardness of the TiSiN system was achieved by silicon that refining the grain size in nano scale and the a-$S_3N_4$ that acts as a barrier to impede dislocation movement [1, 7, 9, 40].

Engineered morphology of the TiSiN thin film also enhances the hardness of the material. By altering the deposition techniques and condition, different morphologies and properties can be obtained. Thornton's classical work described the relationship between the working pressures, the ratio of the substrate temperature to the melting temperature of the depositing compound ($T/T_M$). The

morphology in physical vapor deposition is shown in Figure 2.4 [43, 44].

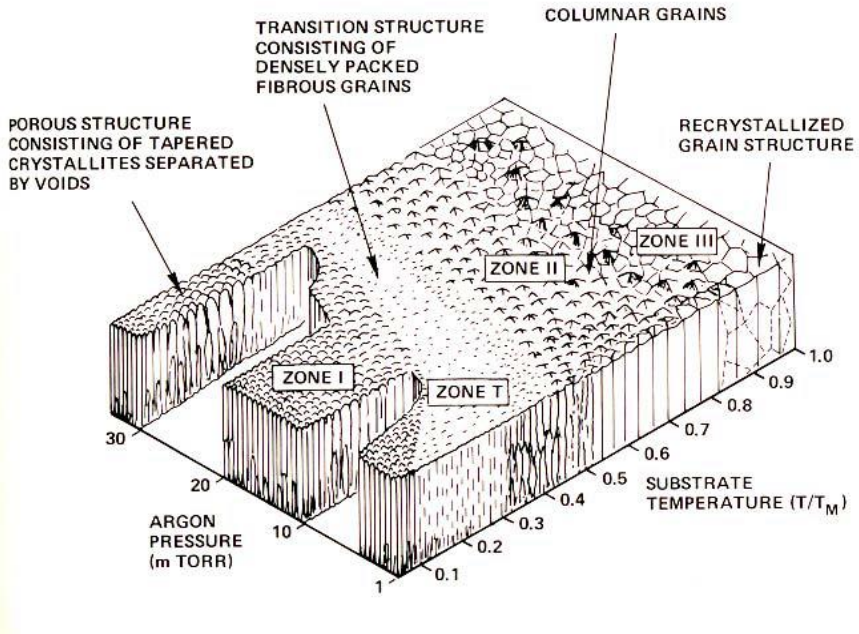


Figure 2.4. Relationship of deposition conditions to film morphology [43, 44]

#### 2.3.2.1 Hardness Enhancement due to Grain Size Reduction

Hall-Petch relation can be applied to study of transition metal silicon nitride, such as titanium silicon nitride, which is the focus of this work. Researchers showed that when silicon is added into titanium nitride during synthesis, titanium nitride grain experiences a significant reduction in size compared to original grain size found in TiN coatings [6, 7, 31, 45-47]. This size reduction limited number of dislocation present in the TiN grain, which lead to less driving force for dislocation to move from one grain to another. This results in reduction of plastic

deformation that in return increases the hardness of the film.

#### 2.3.2.2 Hardness Enhancement due to Spinodal Decomposition and Sharp Interface

Grain size, as discussed in section 2.2.2, will cause decrease in hardness when it reaches below 8-12 nm because of the grain boundary shear. Veprek suggested that during the deposition TiSiN film, if the temperature and driving force for demixing is high enough and diffusion rate is fast, spinodal decomposition occurs, which lead to a formation of fairly regular nanostructure with a single monolayer of a-$Si_3N_4$ and uniform nanocrystalline TiN [1, 29, 35, 40, 48].The single monolayer interface formed by a-$Si_3N_4$ can effectively suppress the grain boundary shear. Figure 2.5 illustrate the structure of nc-TiN/a-$Si_3N_4$.

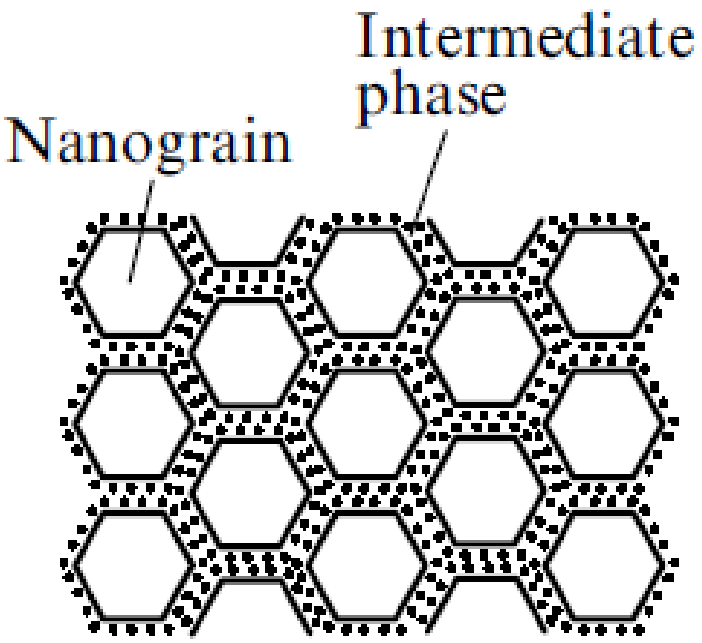


Figure 2.5. Structure of nc-TiN/a-Si3N4 in TiSiN [10]

When titanium, silicon, and nitrogen deposited on the substrate using CVD or PVD, a solid solution of Ti, Si, and N would be formed initially. There are two possible ways of decomposition of a solid solution. If the second derivative of the Gibbs free energy is positive, nucleation and growth occur. This mechanism is not favorable in designing new super hard materials because it forms nanocrystals in different sizes and the formation of the monolayer of interface is not guaranteed. On the other hand, if the second derivative of the Gibbs free energy is negative, spinodal decomposition will occur and result in uniform grain size and sharp interface ($Si_3N_4$) which, according to Veprek, is necessary to produce new super hard materials[1, 2, 6-12, 45-47]. Figure 2.6 shows the Gibbs free energy is

positive, so the second derivative is negative. Thus, according to equation 2, assuming first two terms vanishes due to reference stats. The nc-TiN/a-$Si_3N_4$ system is chemically spinodal even at low nitrogen pressure.

Gibbs free energy of simple binary system A and B is given by Eq. 2:

$$\Delta G_{A_{1-x}B_x} = (1-x)\Delta G_A + x\Delta G_B + \mathrm{RT}[(1-\mathrm{x})\ln(1-\mathrm{x}) + \mathrm{xlnx}] + \mathrm{a}(1-\mathrm{x})\mathrm{x}L_{AB} \qquad (2)$$

Where

$L_{AB}$ is the interaction parameter

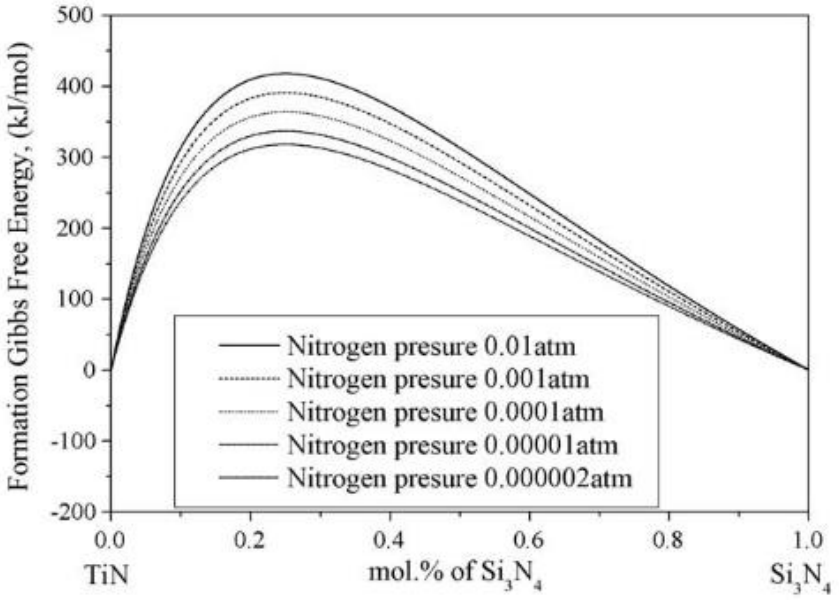


Figure 2.6. Chemical spinodal of the TiSiN system at 873 K for various pressures of $N_2$ gas [10, 49]

Silicon addition in the original TiN is crucial. According to research done previously, silicon is responsible in grain size reduction and nanostructure

refinement [6, 7, 31, 45-47]. The percentage of silicon is also important in reaching super hard TiSiN. In the studies done previously by Veprek, only 1 mono layer thick of the interfacial layer of $Si_3N_4$ can enhance hardness of the material. If the layer is 2 mono layers thick, the benefit of sharp interface would vanish in pure system [24]. Figure 2.7 is an estimation of required percentage of Si to form a monolayer of $Si_3N_4$ at different TiN grain size.

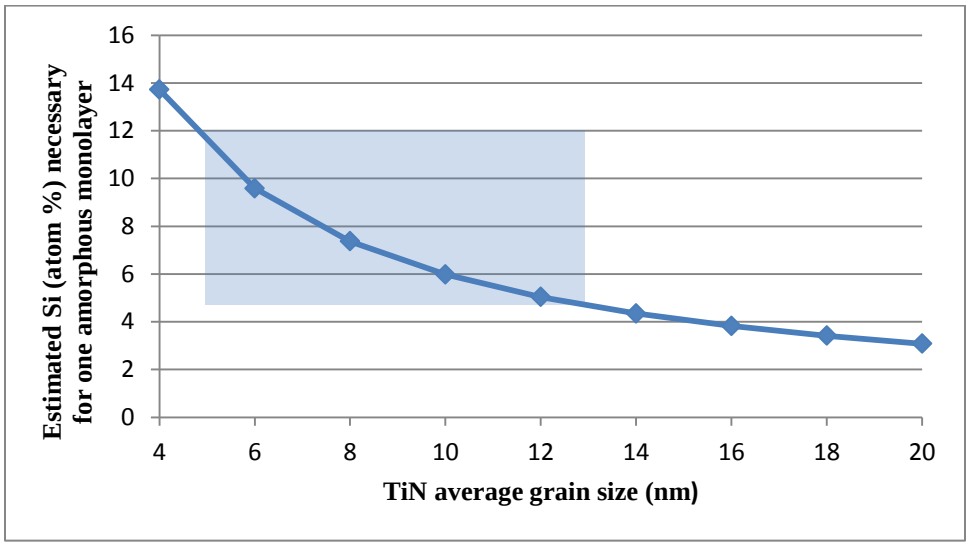


Figure 2.7. Estimated silicon content required forming a ML of $Si_3N_4$ at different grain size of TiN [50]

*2.3.3 Ternary/Quaternary System of TiSiN*

For a long term stable TiSiN with super hardness, the binary system, nc-TiN/a-$Si_3N_4$, is desirable. However, in certain cases, TiSiN may contain an extra amorphous $TiSi_2$ or even another nano-crystalline $TiSi_2$ may be present.

TiSiN with a-$TiSi_2$ shows even higher hardness than the binary ones. In fact, researchers believe that the theoretical hardness of 100 GPa is only achievable using the ternary system. There are a few drawbacks in the ternary TiSiN. First, system is not thermally stable, less oxidation resistant compared to the binary system. Secondly, it is prone to Oswald Ripening, which is a process of small particles dissolve and redeposit onto larger particles due to electronic instability. This would significantly reduce the hardness of the material over time [1, 51].

## 2.4 Titanium Silicon Nitride Hard Thin Film Deposition Techniques

Most often used deposition techniques to synthesize TiSiN are CVD (chemical vapor deposition), and PVD (physical vapor deposition). CVD uses a mixture of target material and volatile precursor. The precursor would act as the carrier for transporting the target material to the surface of the substrate. PVD, on the other hand, uses pure target materials that are vaporized by, for example, laser ablation, and condensed onto the substrate to form thin film. Figure 2.8 shows a sample schematic of a sputtering system.

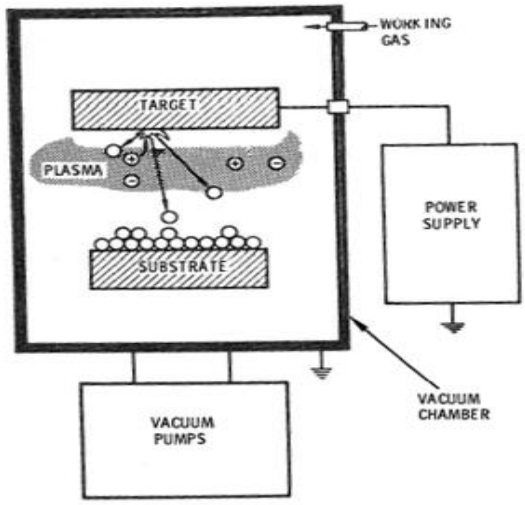


Figure 2.8. Schematic representation of a sputtering system [52]

*2.4.1 Physical Vapor Deposition*

PVD, in large, can be divided into three categories, including sputtering, evaporation and ion plating. Each method has been used for different materials and different applications. R.F Bunshah pointed out three basic steps in coating formation in his book [53]. First of all, target materials need to be vaporized via appropriate method, such as sputtering, vaporization, etc. Second step is transportation of the target materials to the substrate using appropriate means, for example, using plasma. The last step is nucleation and growth of the film [53]. It is worth to mention that in case of TiSiN, spinodal decomposition occurs instead of nucleation and growth.

### *2.4.2 PVD Magnetron Sputtering*

PVD with magnetron sputtering is used to produce film with two major advantages. In magnetron sputtering, a magnetic field is applied at the cathode. The magnetic field can trap electrons to form a highly concentrated region of electrons gathering above cathode. This region would increase the chance of collisions between the electrons and Ar gas, which would result in a higher deposition rate. Another advantage of applying magnetic field at the target is that, by doing so, the bombardment of electrons onto the depositing substrate surface is reduced, which would result in a higher quality deposition [53].

# Chapter 3

# TiSiN SYNTHESIS AND CHARACTERIZATION

TiSiN films in this study were prepared using lab built Reactive PVD Magnetron Sputtering system. Two targets, titanium and silicon, in a nitrogen gas and argon gas mixture were deposited simultaneously onto (001) Silicon wafer. Different characterization techniques were used to analyze the film. Nano-indentation was used to measure the nano hardness of the films. Pin-on-Disk Tribometer and Optical Profilometer were used to measure the coefficient of friction, residual stress, and wear rate of the films. XPS were conducted on some of the films to examine the relationship between mechanical properties and composition of each element. XRD was used to understand the crystal structures and phases difference in different depositing conditions, but not presented in this work.

## 3.1 Reactive Magnetron Sputtering

The TiSiN thin films used in this study were prepared by Jessica Mooney, former graduate student in UT Arlington. The films were deposited on the silicon wafers using lab built PVD magnetron sputtering system, as shown in figure 3-1.

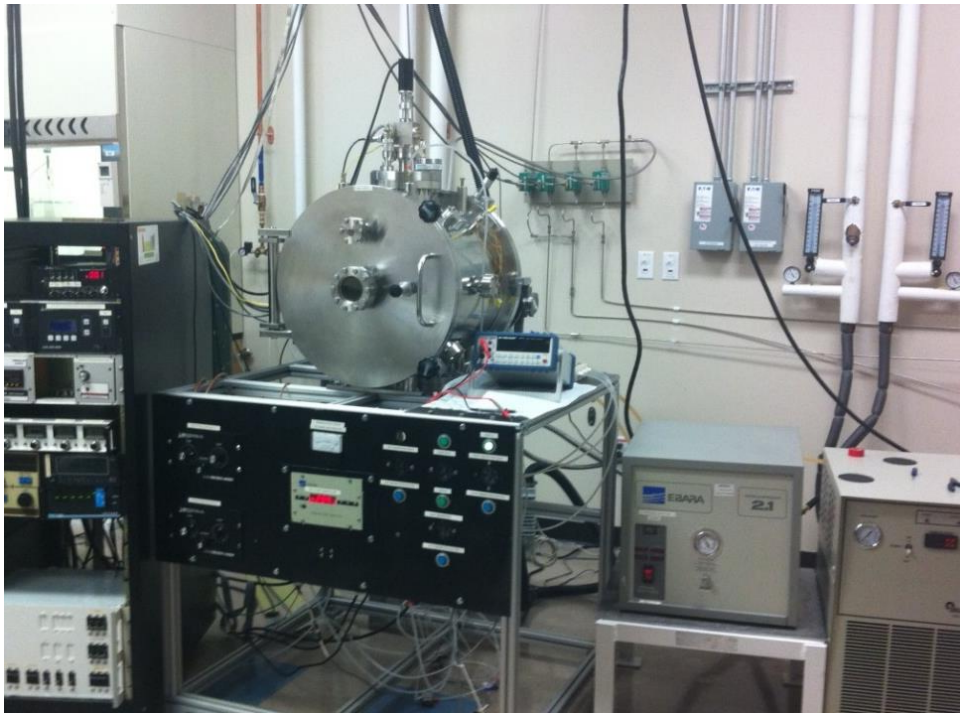

Figure 3.1. Lab built reactive PVD magnetron sputtering systems in SaNEL

The dimension of the cylindrical shaped chamber is 47 cm in diameter and 50 cm in height. Three 2-in magnetron guns, which can hold targets in different thickness including 0.125’’, 0.185’’ and 0.250’’, are mounted in the chamber, where they are pointing directly into the substrate holder, see figure 3.2. This system uses a close loop chilling water system to prevent overheating of the magnetron guns. A pneumatic shutter is fitted to the magnetron guns to shield the target when needed.

Figure 3.2. Photo inside the chamber

The rotatable substrate holder, as shown in figure 3.3, is 10 cm in diameter and can be heated to complement different deposition conditions. The distance of the gun to the substrate holder can be adjusted. An open loop filtered tap water supply is connected to the substrate holder rotating device to keep the temperature low.

Figure 3.3. Substrate holder used in lab-built reactive PVD magnetron sputtering system

A detailed schematic of the system is shown in Figure 3.4. This system has the capability to reduce the internal pressure in the range of $10^{-7}$ Torr. First, a rough pump with a molecular sieve trap brings the pressure in the chamber down to 20 mTorr. Then a cryo pump connected with a cryo compressor pumps out the remaining air and humidity to reach a high vacuum. When the base vacuum of $10^{-7}$ Torr is reached, various gases can be vented into the chamber, such as argon gas, methane gas, oxygen, or nitrogen as needed. The flow rate of gas mixture can be controlled using mass flow controllers that are connected to each gas supplied pipe.

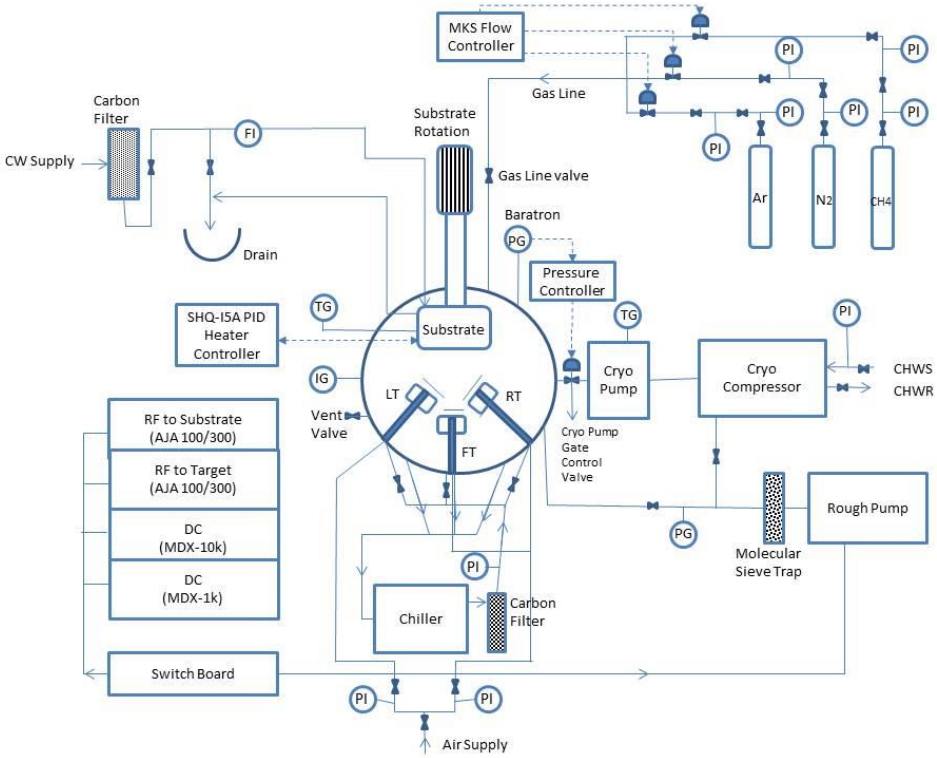


Figure 3.4. Schematic of reactive PVD magnetron sputtering system [50]

DC and RF power from the power source, as shown in Figure 3.5, can be applied to any of the three magnetron guns or substrate holder depending on design of the experimental conditions.

Figure 3.5. Photo of power supplies and control panels used by reactive PVD magnetron sputtering system

## 3.2 TiSiN Film Deposition Conditions and Setups

Experimental deposition conditions were selected to examine and to understand the impact on the properties of the TiSiN by altering sputtering parameters such as the bias on the substrate, rotation speed of the substrate holder, and power applied to Silicon target. When using PVD system to synthesize TiSiN thin film, it is crucial to reduce the pressure in the chamber down to a range of

$10^{-7}$ Torr, because a slightest amount of oxygen may severely reduce the properties of the film. In the SaNEL system, this was made possible with a rough pump which brings the pressure down to 20 mTorr, and then a cryo pump with cryo compressor creates a vacuum within the range of $10^{-7}$ Torr. Two targets, Silicon and Titanium, were installed into the chamber onto the magnetron guns and a mixture of Nitrogen gas and Argon gas were filled in the chamber. In previous studies, it was suggested that Nitrogen gas up to 13-20% of the total mixture is optimal. 20% $N_2$ and 25% $N_2$ were used to synthesize TiSiN film in this study. A negative bias is applied to the substrate holder in order to reject oxygen ions that might otherwise incorporate itself in the coating, 100 V bias, 200 V bias, 300 V bias, and 500 V bias were used in this study to understand how bias affects properties of the films. Substrate holder was rotated to ensure the materials deposited onto the wafer were uniform. Three different speeds (1 RPM, 3 RPM，6 RPM ) were used in this study. Gun distance was set at 10.5 cm from the surface of the substrate to the target materials. For all studies, the substrate was heated up to 550 ℃ to ensure the formation of desired morphology. Detailed deposition conditions of the samples are listed in table 4.1.

## 3.3 Characterization of TiSiN Thin Film

Multiple scientific instruments were used in characterizing TiSiN films in details. XRD was used to determine the crystal structure and phases. XPS was

used to determine the composition of the film on the surface. Pin-on-Disk Tribometer was used to measure the coefficient of friction and create wear track on the surface of the film. Optical Profilometer was used to measure the residual stress and wear rate of the films.

### *3.2.1 XRD*

Bruker D-8 Advance X-Ray Diffractometer with a Cu Kα radiation was used in the study of the TiSiN thin film. Data used in this study was obtained by Jessica Mooney, former graduate student at UT Arlington [50]. Wavelength of radiation of the Bruker D-8 is 1.54 Å. All results were obtained with voltage and filament current at 40 kV and 40 mA, respectively, at both θ-2θ and low angle detector scan. Dwell time was set at 2 seconds and a small step size of 0.03 °was incorporated to obtain a high resolution result[50]. Thus obtained results were plugged in Equation 3.1 to calculate the grain size of the film. The result is not discussed in this work.

Eq. 3.1: Scherrer Formula for Estimation of Grain Size

$$\tau = \frac{K\lambda}{\beta cos\theta}$$

Where

K is the shape factor

λ is the wavelength of the X-ray, 1.54 Å in this case

β is the FWHM(full width half maximum)

θ is the Bragg's angle of diffraction

### *3.2.2 Nanoindentation*

Hardness of the TiSiN thin films were measured by Hysitron Uni 1 Nanoindenter. The hardness of the TiSiN film were measured by Jessica Mooney, former graduate student at UT Arlington [50]. Cubic corner tips were used in the experiment. The surface roughnesses of the films were detected first with the indentation instrument, and then areas with the smoothest surfaces were chosen to get indented. Indentation depths have to be less than 10% of the total thickness of the thin film, which was measured using optical Profilometer. The hardness and elastic modulus were recorded for 9 indentations in 20x20 micrometers.

### *3.2.3 Tribological Test*

Coefficients of Friction (COF) are measured using Pin-on-Disk tribometer in SaNEL (surface and nano engineering lab). A wear track was also created during the test for wear rate analysis using Optical Profilometer. Alumina ball with 1/4 inches diameter was chosen to be the counter material for the wear test. Test conditions were set at 400 m in sliding distance, using 10 cm/s as the linear speed, and 1N as the load. Wear rates were calculated using equation 3.2. The areas of

the wear track cross section were obtained using Optical Profilometer. The average of four values that were collected at different points of the track was used in the calculation.

Equation 3.2:

$$\text{Wear Rate} = \frac{Average\ of\ Wear\ Track\ Cross\ Section\ Area * Circumferece\ of\ the\ Track}{Load * sliding\ distance}$$

*3.2.4 Optical Profilometer*

The thickness, residual stress, and cross sectional areas of the wear track were determined by using Veeco NT-9100. 5x, 20x, 50x objectives were available to use, but only 5x objective was used in this study. Thickness of the films was obtained by measuring the step from the surface of the thin film to the non-deposited surface of the substrate. Cross sectional areas of the wear track were obtained using the 2-Dimensional feature, where data can be extracted as text file, plotted using Origin software. Data collected could also be used to measure the residual stress that presents in the film. There is a residual stress present in the film, which will induce a curvature difference between the original substrate wafer and the wafer with coating. By using the Stoney's equation, Eq 3.3, residual stress would be estimated.

Equation 3.3:

$$\sigma_f = \frac{E_s d_s^2}{6(1 - v_s)} * \frac{1}{d_f} * \frac{1}{R}$$

### *3.2.5 SEM and EDS*

Surface and cross sectional morphology, and compositional analysis of the films were conducted using a Hitachi S-3000N Variable Pressure SEM with an attached EDS and a Hitachi S-4800 SEM. Experiments were conducted using a working distance of 15mm and 20-25 KeV was used as the voltage setting.

### *3.2.6 XPS*

Surface composition of the TiSiN thin films were characterized using Perkin-Elmer Phi 560 XPS/Auger system with an Al Kα source and a characteristic voltage of 1253.6 eV. Data used in this study were obtained by Yishu Wang, graduate student at UT Arlington. In order to remove extra contaminations such as Oxygen and Carbon on the surface of the TiSiN film, Argon was used to sputter the surface of the samples for a few minutes.

# Chapter 4

# RESULT AND DISCUSSION

Since the development of TiC in the 60s' and TiN's appearance 20 years after that, scientists have spent enormous amount of time and efforts in developing a new era of coating materials that would possess higher hardness , higher wear resistance and higher oxidation resistance. Scientist have discovered that by adding Silicon into TiN, the hardness increased significantly from 20 GPa to 70 GPa and the oxidation resistance from 450 ℃ to 600 ℃ [1, 3, 4]. The hardness enhancement is due to the grain size reduction and unique morphology suggested by scientists [1, 6-10, 43-45]. It is believed that upon high temperature (>=550 ℃) spinodal decomposition would occur when the material was deposited onto a substrate. A binary phase consists of nano crystalline TiN and amorphous $Si_3N_4$. One reason that TiSiN can obtain a theoretical hardness of 100 GPa is that the addition of Si may reduce the grain size of the TiN, and according to Hall-Patch relation, this would increase the hardness of the material by reducing number of dislocation per grain. Another reason for the hardness enhancement is that the amorphous $Si_3N_4$ would form a mono layer of sharp interface that surround the TiN nano grain in order to impede dislocation movement.

In this study, the films tested were prepared using lab-built PVD reactive magnetron sputtering system by Jessica Mooney, former graduate student at UT

Arlington. In setting up the experiment, it is important to understand that the impact of existence of oxygen to TiSiN would significantly reduce the mechanical properties of the film [54]. In order to prevent the oxygen to get into the TiSiN, a negative bias was applied on the substrate to repel the oxygen during the deposition. At the same time, low pressure around 5 mTorr was stabilized to limit the presence of oxygen and other impurities. 5 different biases (100 V, 200 V, 300 V, and 500 V) were chosen as variables in deposition conditions to understand the effects of increasing energy presence at the substrate on mechanical properties because substrate bias may have an impact on the refinement of the nanostructure. Gas mixtures of nitrogen and argon were continuously supplied into the chamber consisting nitrogen gas and argon gas, the ratios of $Ni_{2:}$ Ar were 1:4 and 1:5. The substrate was heated to 550 ℃ to ensure activation of spinodal decomposition and the formation of nc-TiN/a-$Si_3N_4$. Meanwhile, the substrate holder was rotated during the deposition process, so the materials sputtered onto the surface of the wafer would be uniform. Three rotation speeds (1 RPM, 3 RPM, and 6 RPM) were used to study the effects of rotation speed on mechanical properties and wear behaviors. For all deposition, the magnetron guns were place 10.5 cm away from the surface of the substrate. Constant power of 150 W was applied to the Titanium target by adjusting voltage and current. Three different power settings (50 W, 55 W, and 60 W) were applied to Si target. The deposition conditions and hardness are listed in Table 4.1. Experimental conditions were changed in terms

of substrate bias, rotation speed, power on Si target, and nitrogen composition in the gas mixture in the chamber.

Table 4.1. Record of TiSiN deposition conditions [50]

| | Substrate | | | Ti Target | | | Si Target | | | Volumetric Flow | | Deposition Rate (nm/h) |
|---|---|---|---|---|---|---|---|---|---|---|---|---|
| Coating Name | Power (W) | Voltage (V) | Current (mA) | Power (W) | Voltage (V) | Current (mA) | Power (W) | Voltage (V) | Current (mA) | Ar (sccm) | $N_2$ (sccm) | |
| B100 Si60 | 3.8 | 100 | 38 | 150 | 307 | 537 | 60 | 263 | 228 | 20 | 5 | 390 |
| B200 Si65 | 8 | 200 | 40 | 150 | 328 | 501 | 65 | 266 V | 244 | 20 | 5 | 380 |
| B300 Si65 | 12.6 | 300 | 42 | 150 | 327 | 503 | 65 | 267 V | 243 | 20 | 5 | 335 |
| B500 Si65 | 19.5 | 500 | 39 | 150 | 333 | 492 | 65 | 264 V | 246 | 20 | 5 | 230 |
| | | | | | | | | | | | | |
| B100 Si50 | 3.9 | 100 | 39 | 150 | 318 | 519 | 50 | 255 V | 196 | 20 | 5 | 390 |
| B100 Si55 | 3.7 | 100 | 37 | 150 | 321 | 510 | 55 | 248 V | 222 | 20 | 5 | 380 |
| B100 Si60 | 3.8 | 100 | 38 | 150 | 307 | 537 | 60 | 263 V | 228 | 20 | 5 | 390 |
| B100 Si60 N25 | 3.7 | 100 | 37 | 150 | 315 | 522 | 60 | 265 V | 226 | 18.75 | 6.25 | 390 |
| | | | | | | | | | | | | |
| B100 Si60 N25 1RPM | 3.9 | 100 | 39 | 150 | 322 | 510 | 60 | 263 | 228 | 18.75 | 6.25 | 390 |
| B100 Si60 N25 3RPM | 3.7 | 100 | 37 | 150 | 315 | 522 | 60 | 265 V | 226 | 18.75 | 6.25 | 390 |
| B100 Si60 N25 6RPM | 3.7 | 100 | 37 | 150 | 323 | 509 | 60 | 253 | 237 | 18.75 | 6.25 | 385 |

## 4.1 Effect of Bias on Mechanical Properties of TiSiN

Four different biases (100 V, 200 V, 300 V, and 500 V) were applied when depositing TiSiN. Wear test, optical profilometer, SEM, and XPS were used to determine the coefficient of friction and wear resistivity. It is important to mention that the sample prepared with 100 V bias was synthesized with 60 W power applied to silicon target, and the other three were synthesized with 65 W power applied to silicon target. In order to interpret and understand the results of the analysis, which was done by Jessica Mooney, former graduate student at UT Arlington, was incorporated in this study. Analyses performed by Jessica include XRD, nanoindentation, surface roughness and residual stress calculation.

Hardness test were performed by Jessica Mooney using nanoindentation. Tribological wear tests were performed on 100 V, 200 V, 300 V, and 500 V bias to assess the effects of increased substrate bias on the COF (coefficient of friction) of the TiSiN films, as shown in Figure 4.1 to Figure 4.4. As mentioned in chapter 3, alumina balls with 1/4 inch were used as counter materials (hardness of alumina is around 20.5 GPa).The TiSiN film were glued to a stainless steel sample holder, and wear tests were performed in a dry atmosphere at room temperature. The load applied to all four tests was 1 N and the linear sliding speed was set at 10 cm/s. Wear tracks were then assessed using optical profilometer to obtain a 2-D and 3-D profiles. The cross sectional areas of the wear tracks were

calculated using Origin software, as seen in figure 4.5 to figure 4.8. 2-D and 3-D wear track obtained using optical profilometer are shown in Figure 4.9-4.13. Test results are listed in Table 4.2.

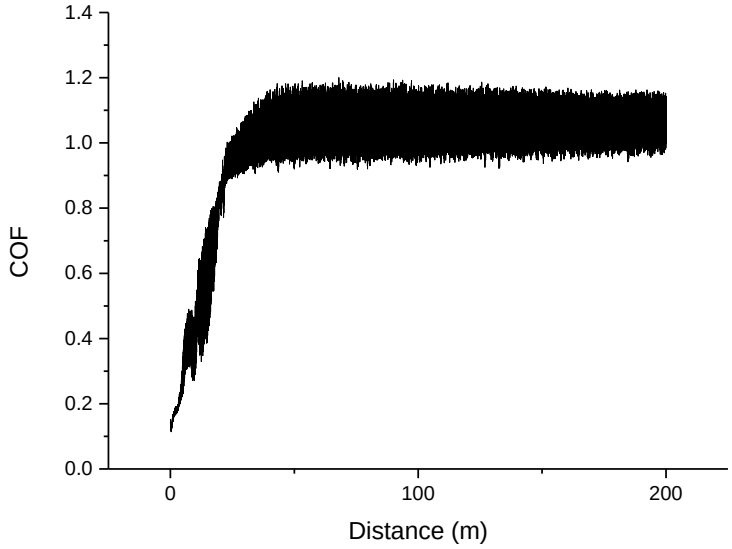


Figure 4.1. COF of 100 V bias with 60 W Si power

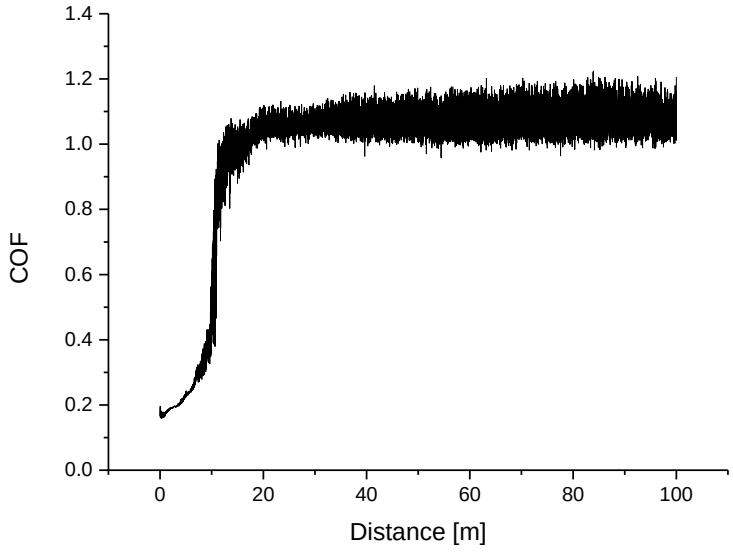


Figure 4.2. COF of 200 V bias with 60W Si power

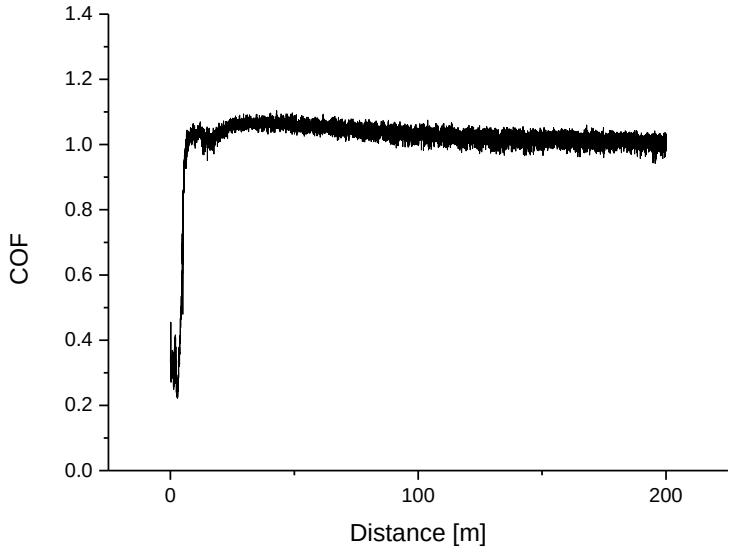


Figure 4.3. COF of 300 V bias with 60 W Si power

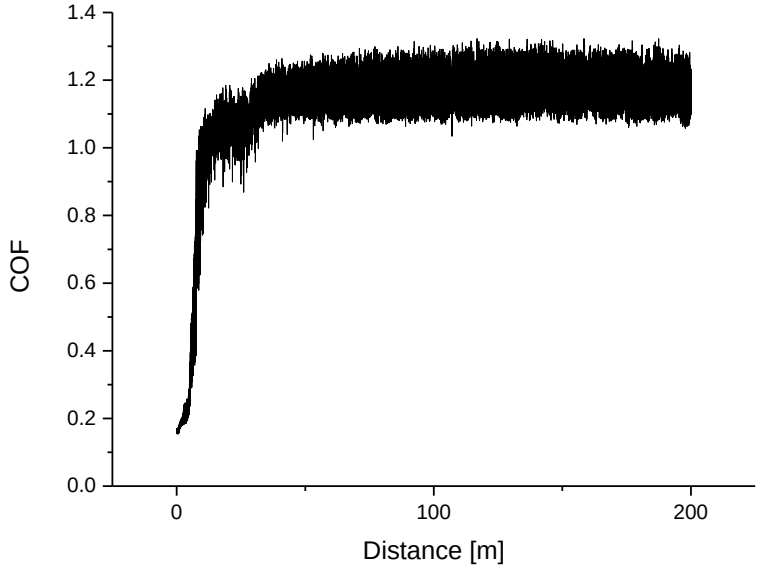


Figure 4.4. COF of 500 V bias with 60 W Si power

COFs of TiSiN reported in previous studies showed a large variation, ranging from 0.15 up to 1.0 [55]. These fluctuations of COFs are assumed to be caused by silicon content within the film. It was understood that a small amount of silicon (lower than 1%) may reduce the coefficient of friction of an alloy. However, a reverse effect was observed at high silicon content [56]. Other studies on the tribological behavior of TiSiN film also concluded that COFs increase as silicon content increases, and a high COF of near 1.0 was observed at around 10% of silicon. XPS was applied to analyze the amount of silicon in these samples. As shown in figure 4.5, silicon content in the film was 25.71%. This may explain the high COFs obtained in this study.

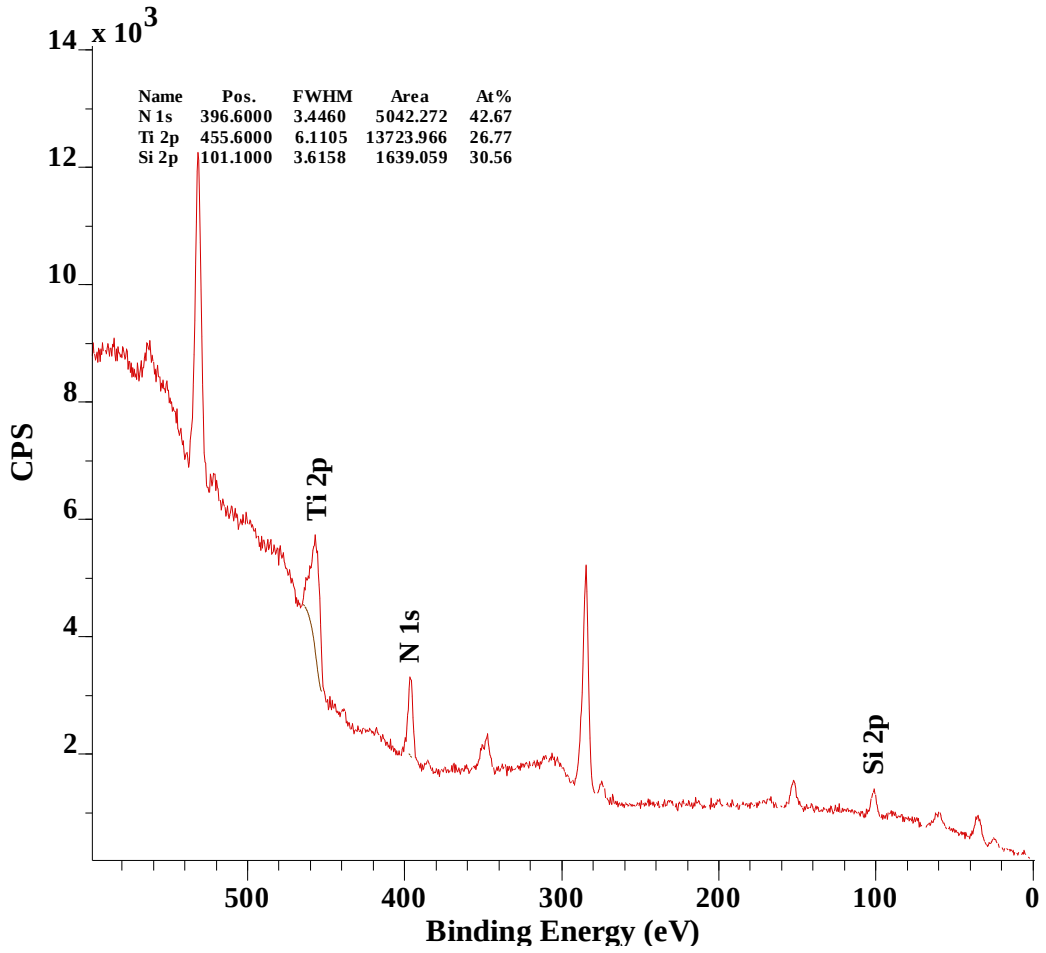


Figure 4.5. XPS result of TiSiN 100 V bias and 60 W Si power

From the data shown above, it is obvious that as the bias applied to the substrate increases, the hardness of the films decreases significantly. Many studies suggested that increasing bias would allow less texture in film, and therefore should enhance hardness. The reduction in hardness was assumed to be caused by excessive bombardment of the ions during the deposition, which result in destruction of the microstructure.

Figure 4.6 to figure 4.9 are the 2-D profile generated using origin software. The width of the wear track increased as the bias increased. Because the shape of each sample was different due to other characterization performed on the sample. Different radiuses were utilized for each test. 100 V sample had radius of 6mm and sliding distance of 400 m. The width of the track was 180 μm and depth was .327 μm. 200 V sample had a sliding distance of 100 m, because the film was thinner compared to other samples. Less sliding distance was applied to prevent the worn out of the TiSiN coating. Radius was set at 7 mm. The width and depth of the track were 172 μm and 0.246 μm, respectively. Due to the decrease of the hardness, 200 m sliding distance was applied to 300 V and 500 V samples. Track width of both samples increased to around 190 μm compared to samples with lower bias. Radiuses of the track of these two samples were 19 mm and 10 mm, respectively. Wear rates of the samples are recorded in Table 4.2. Samples with higher bias appear to have high wear rates. Relationships of bias to hardness, COF, and wear rate were recorded in figure 4.6.

Table 4.2. Tribological experiment conditions and results of TiSiN varying substrate bias

| Bias(-V) | Wear Track Radius (mm) | Wear Track Width (μm) | Wear Track Depth (μm) | Wear Rate ($mm^3/N*m$) | COF | Hardness [50] |
|---|---|---|---|---|---|---|
| 100 | 6 | 180 | 0.324 | 7.90E-06 | 1.10 | 37.1 |
| 200 | 7 | 172 | 0.246 | 9.2E-06 | 1.10 | 32.2 |
| 300 | 19 | 192 | 0.285 | 2.12E-05 | 1.01 | 31.5 |
| 500 | 10 | 190 | 0.796 | 2.95E-05 | 1.08 | 18.5 |

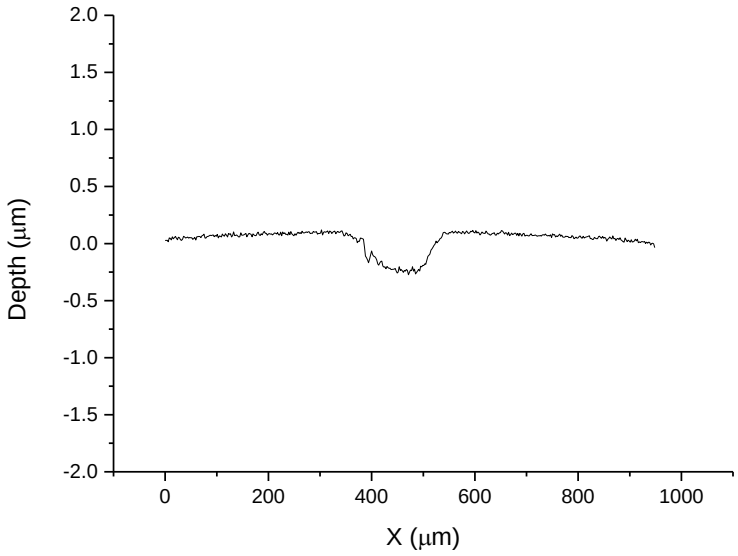


Figure 4.6. 2-D wear track of 100 V TiSiN plotted in Origin

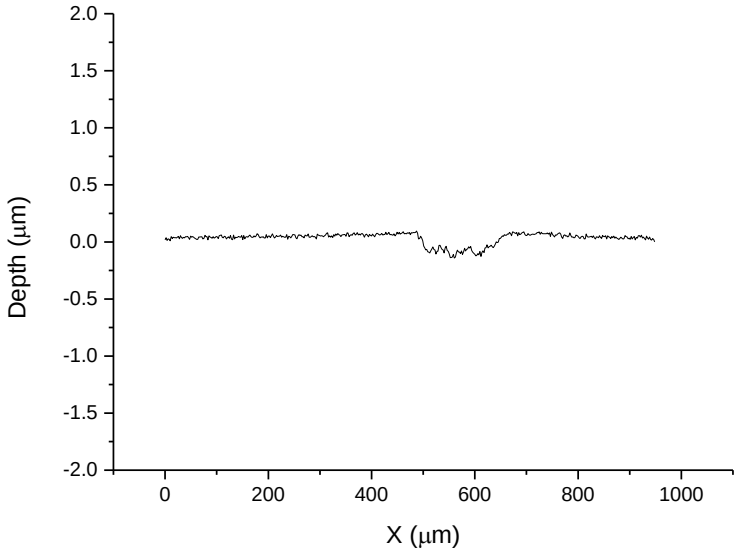


Figure 4.7. 2-D wear track of 200 V TiSiN plotted in Origin

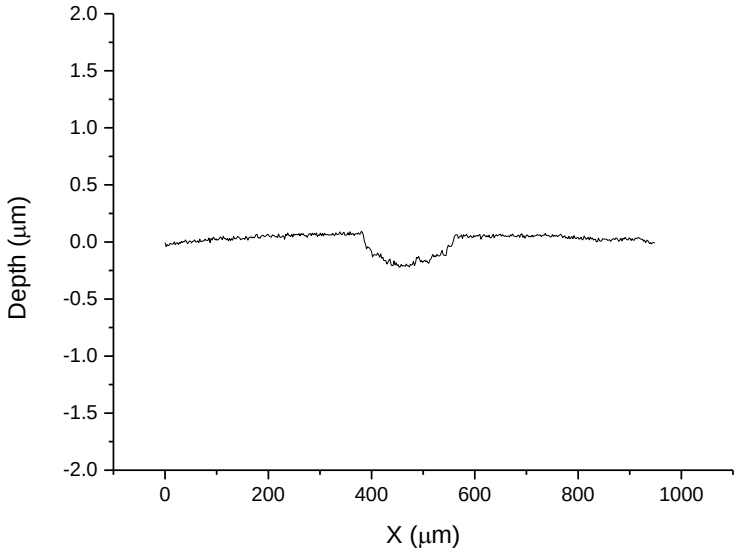


Figure 4.8. 2-D wear track of 300 V TiSiN plotted in Origin

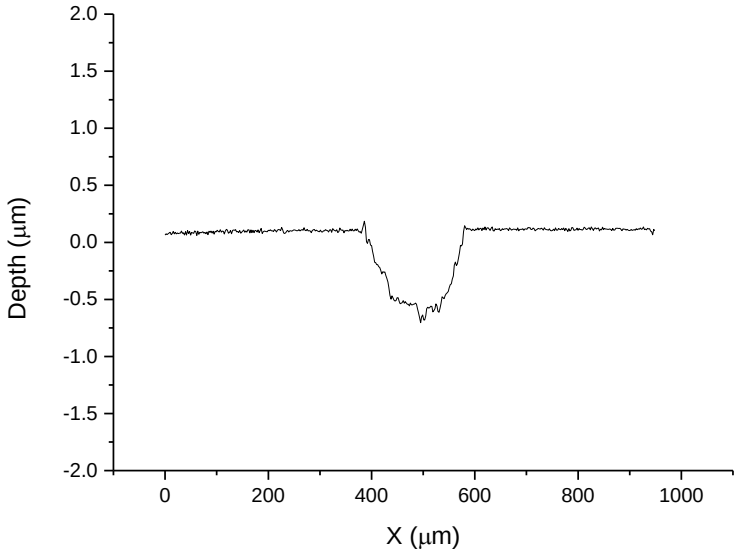


Figure 4.9. 2-D wear track of 500 V TiSiN plotted in Origin

It was expected that with the increase in the hardness of the film, wear rate

decreases, and better wear behavior would be observed. These Two-dimensional images and three-dimensional images of the wear track of 100 V, 200 V, 300 V, 500 V were obtained using optical profilometer are shown in figure 4.10 to 4.13.

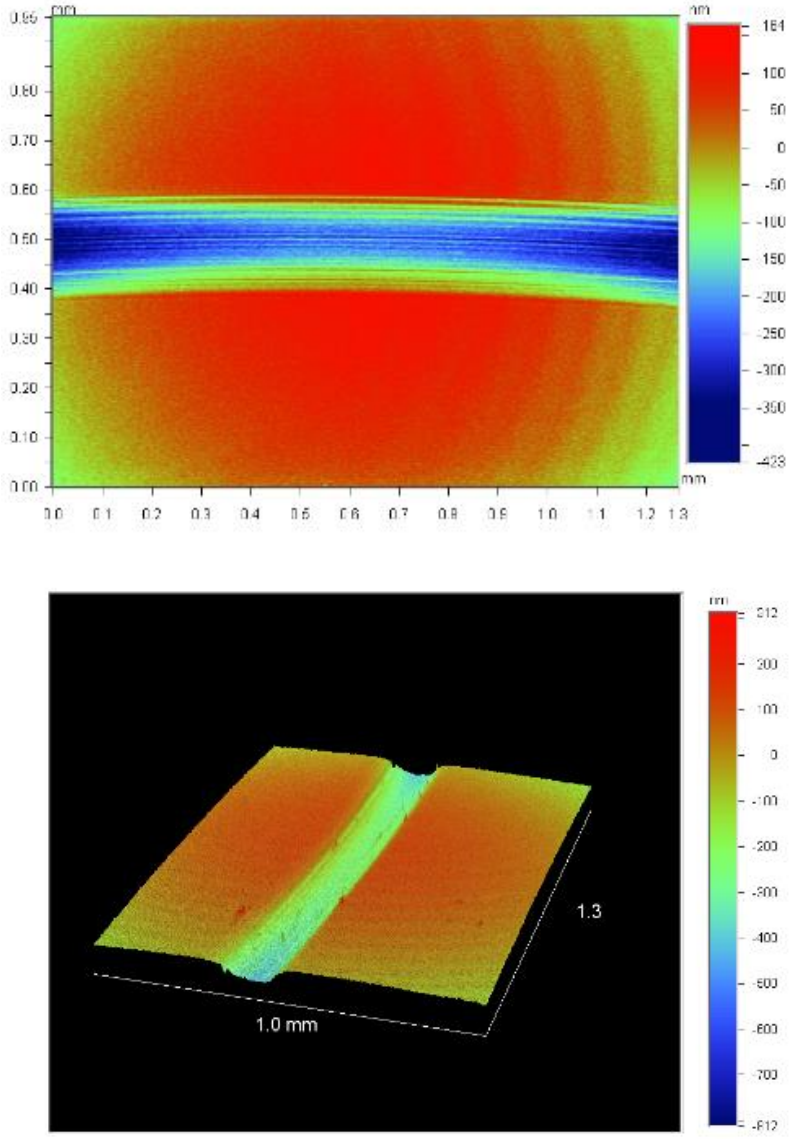


Figure 4.10. 2-D and 3-D wear track of TiSiN 100 V bias

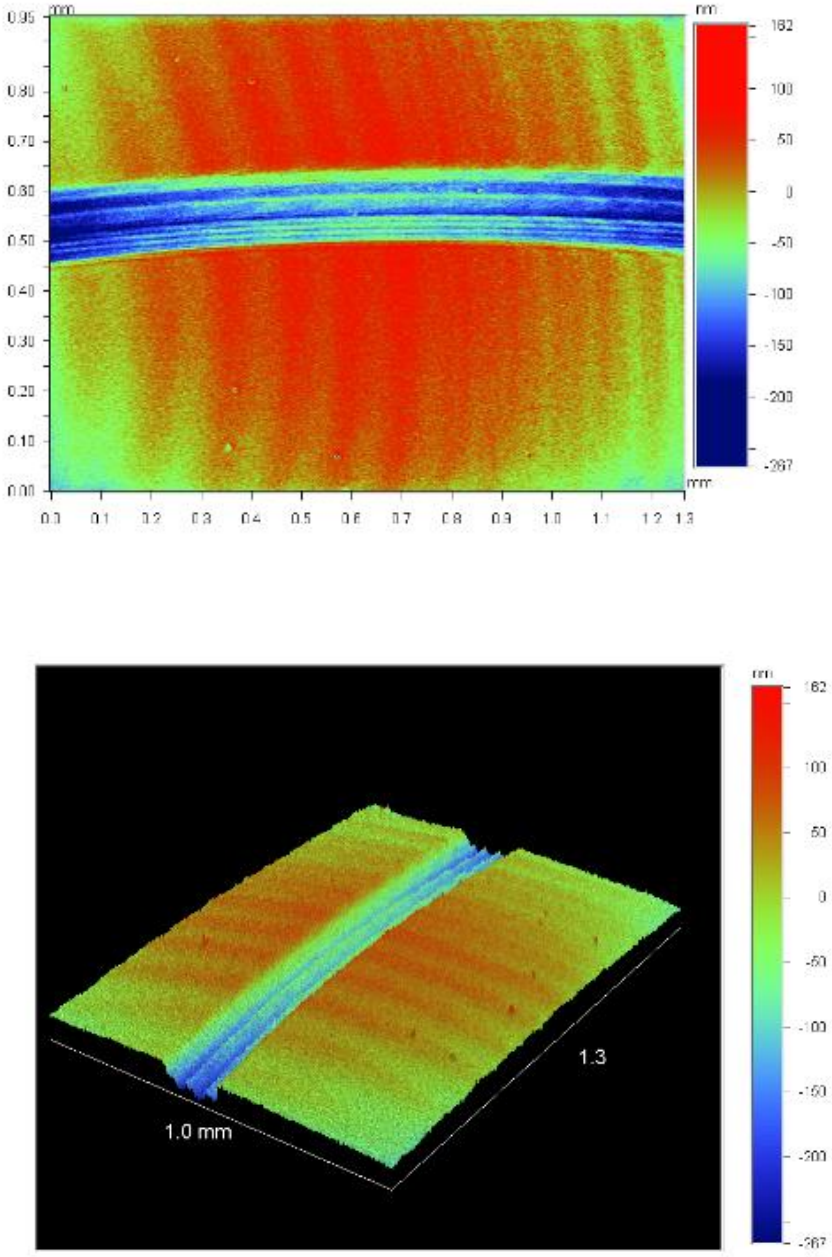


Figure 4.11. 2-D and 3-D wear track of TiSiN 200 V bias

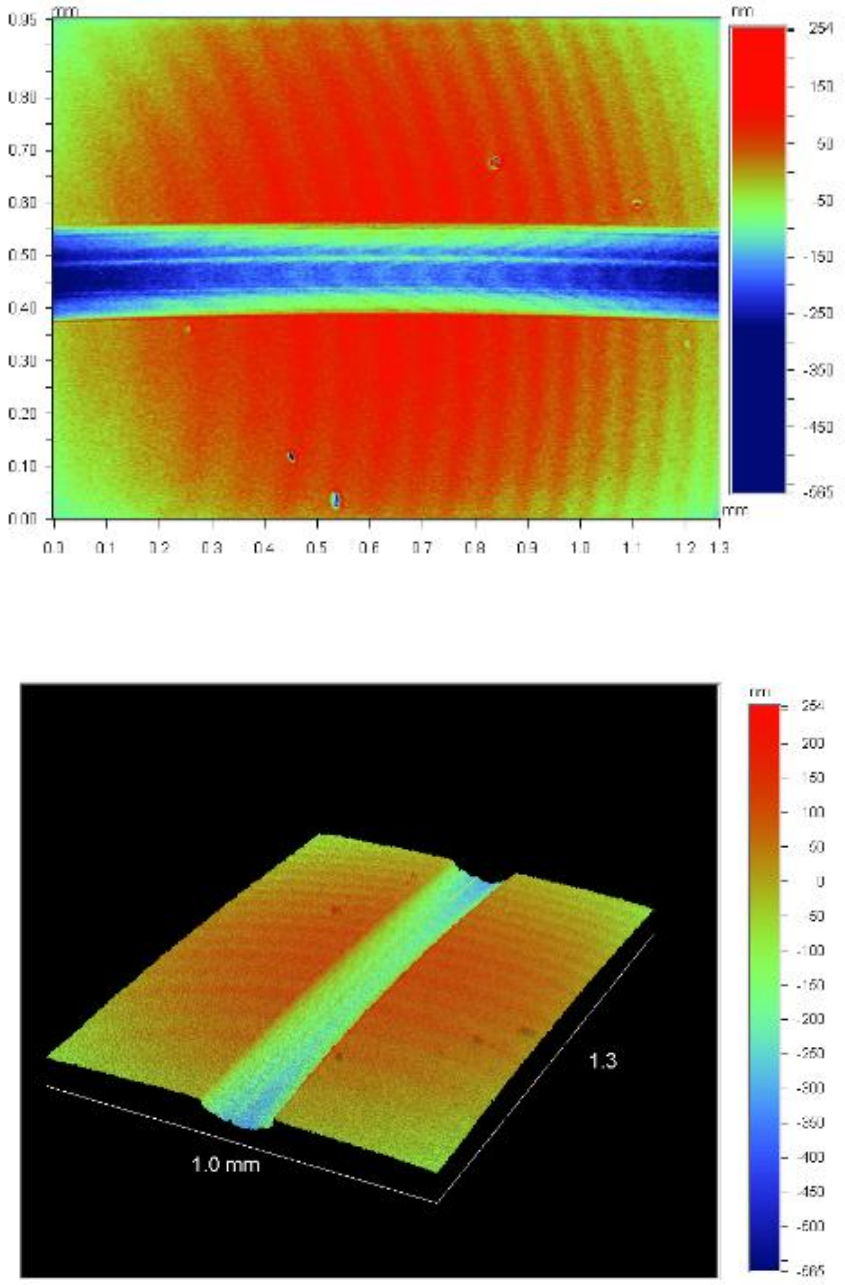


Figure 4.12. 2-D and 3-D wear track of TiSiN 300 V bias

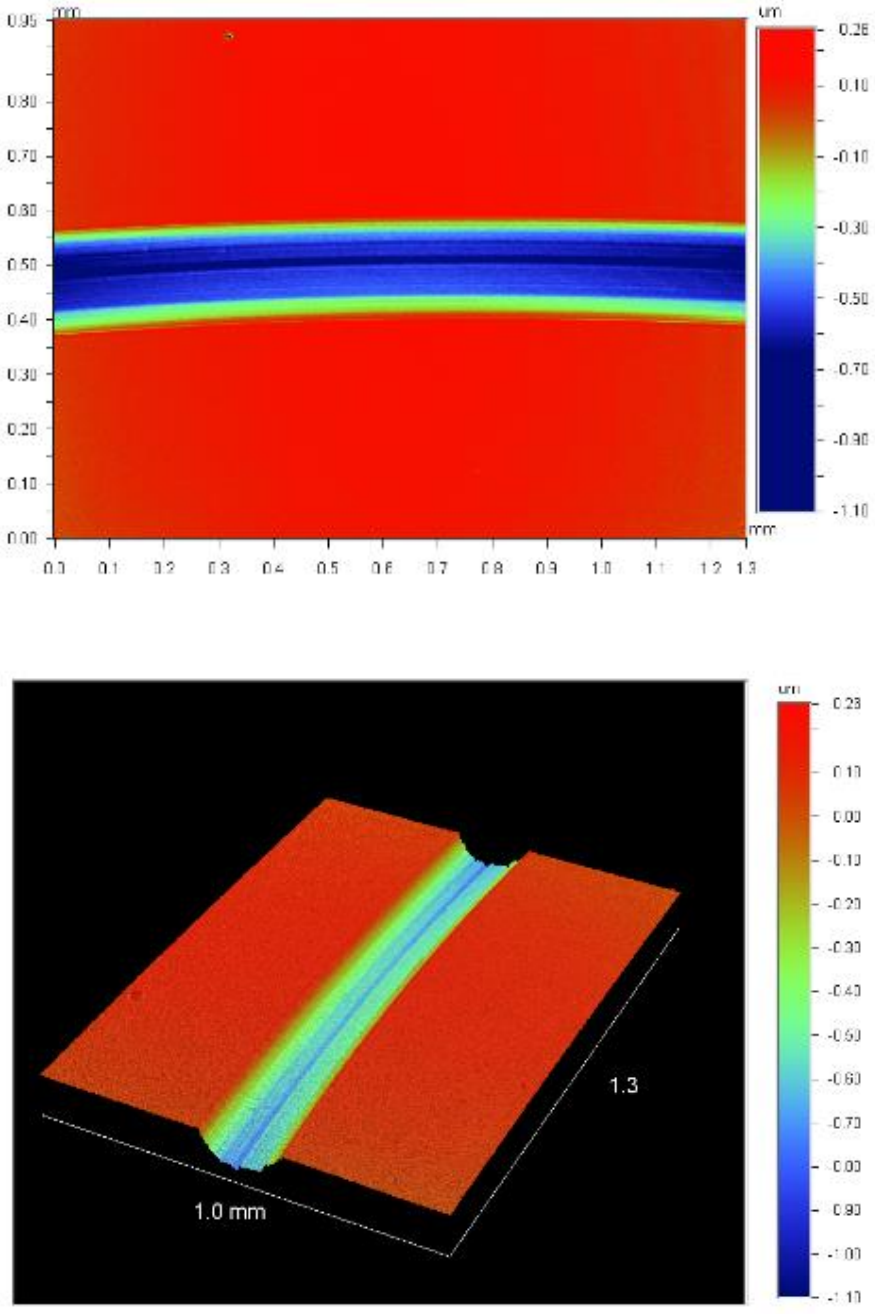


Figure 4.13. 2-D and 3-D wear track of TiSiN 500 V bias

Irregular wear tracks were observed in the 100 V bias coatings. It can be seen in figure 4.1; small spikes appear in the wear track. It was assumed that the spikes were the debris of the counter materials, and in this case, alumina balls. Because the coating can be as hard as 35 GPa or higher, and the hardness of the alumina ball is 20.5 GPa, this may result in a three body wear where the debris of the alumina balls act as another party in the wear process that led to higher wear rate for TiSiN with a high hardness of 35 GPa or higher. Figure 4.14 and 4.15 shows a SEM image of possible debris of alumina on the wear track. Nevertheless, from the results obtained above and plotted in Figure 4.16, film with higher hardness still performed better in terms of wear rate.

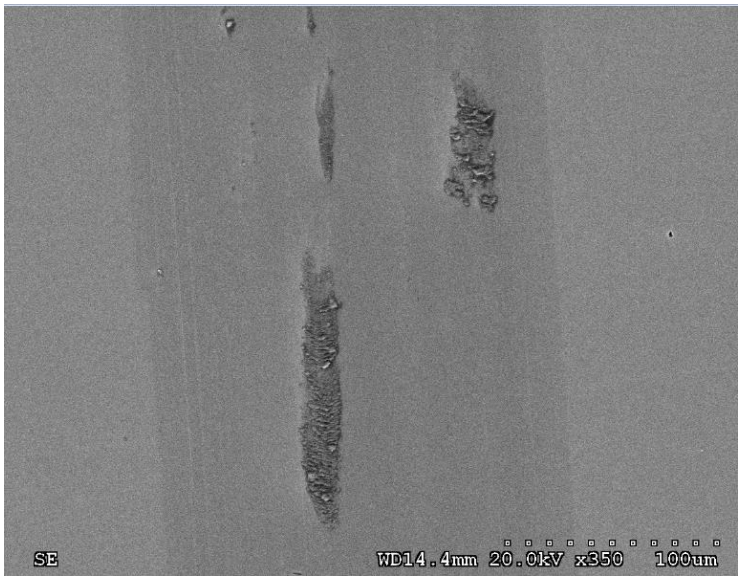


Figure 4.14. SEM image of wear track on TiSiN 100 V bias

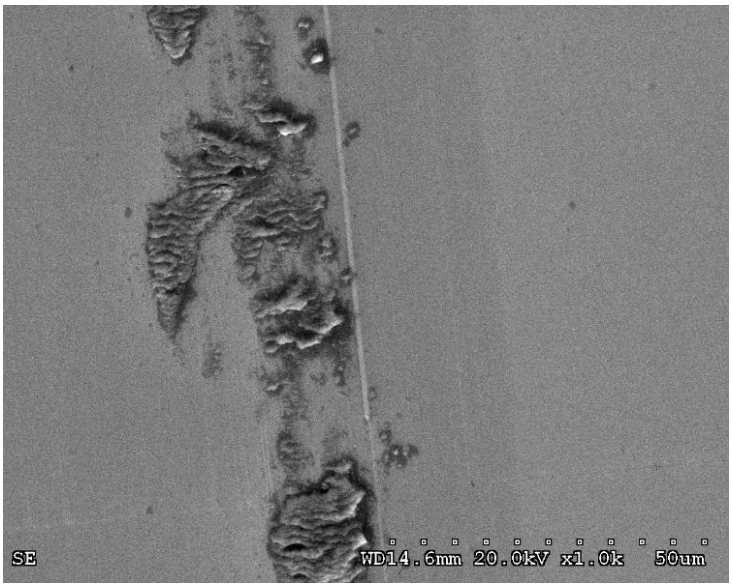


Figure 4.15. SEM image of wear track on TiSiN 100 V bias

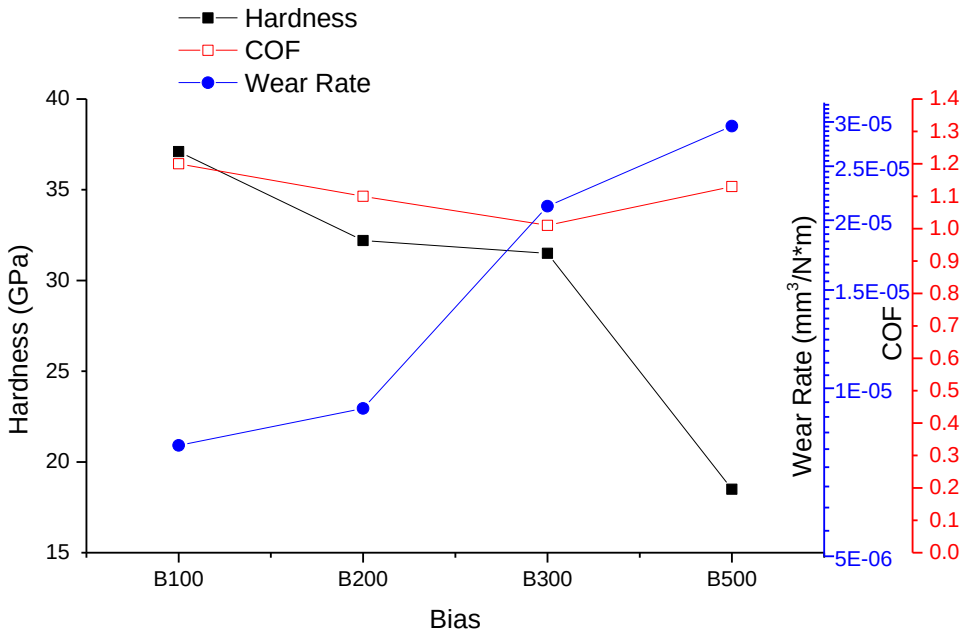


Figure 4.16. Effect of bias on hardness, wear rate, and COF.

## 4.2 Effect of Power applied to Silicon Target and Nitrogen Content in the Gas Mixture on Mechanical Properties of the TiSiN

From 4.1, we found that TiSiN deposited with PVD reactive magnetron sputtering with different bias applied to the substrate holder displays different hardness and wear behaviors. From figure 4.16, we concluded that 100 V bias produced hardest sample with highest wear resistance. In this experimental section, the power applied to silicon target and the composition of nitrogen in the gas mixture were altered in order to explore the best condition to produce film with higher hardness and better wear resistance.

Three power conditions (50 W, 55 W, 60 W) were used in the study. Tribological wear tests were performed on samples produced with 50 W, 55 W, 60 W Si power and sample prepared with 60 W Si/25%$N_2$ to assess the effect of increased power on Si target to the COF (coefficient of friction) of the TiSiN films, as shown in Figure 4.1 and Figure 4.17 to 4.19. All samples were prepared at three RPM and 100 V bias to the substrate holder. Test conditions were the same as indicated in last experimental section. 1 N load was applied on the pin that holds an alumina balls with 1/4 inch, and wear tests were performed in a dry atmosphere at room temperature with 10cm/s linear speed. Test results are listed in Table 4.4.

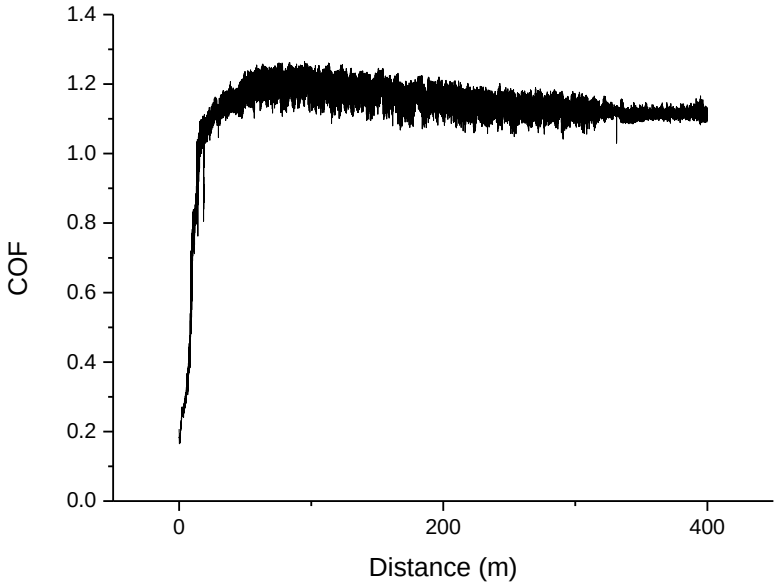


Figure 4.17. COF of TiSiN with 100 V bias, 50 W Si and 20% $N_2$

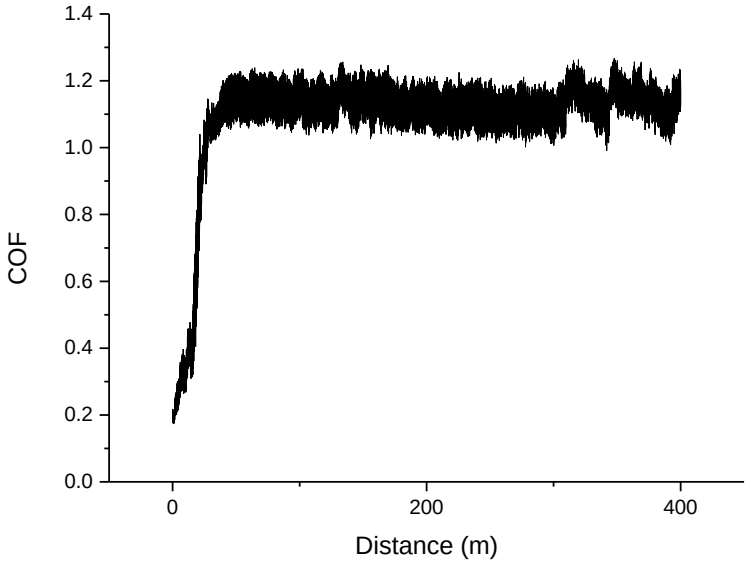


Figure 4.18. COF of TiSiN with 100 V bias, 55 W Si power and 20% $N_2$

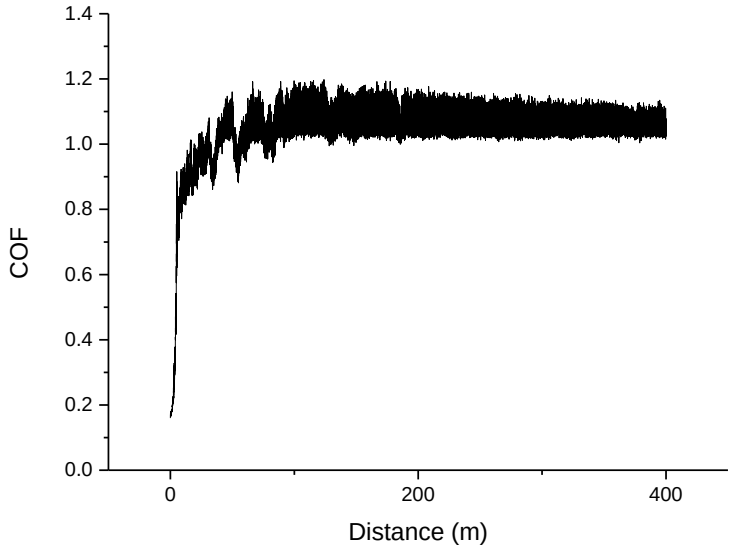


Figure 4.19. COF of TiSiN with 100 V bias, 60 W Si power and 25% $N_2$

Hardness of these samples was measured using nanoindentation as described in chapter 3. The hardness, wear track width, depth, wear rate, and COFs are listed in Table 4.4. XPS was applied to analyze the amount of different elements in these samples. As shown in table 4.3, silicon content increases as power applied to silicon target increases. The high content of silicon in the film may be the cause of the high coefficient of friction observed in the tribological test as discussed in section 4.1.1.

Table 4.3. XPS results of TiSiN with different silicon target power and $N_2$ content

| Sample | N 1s | Ti 2p | Si 2p |
|---|---|---|---|
| 100V B 50W Si | 46.62% | 29.08% | 24.3% |
| 100V B 55W Si | 49.79% | 25.18% | 25.03% |
| 100V B 60W Si | 42.67% | 26.77% | 30.56% |
| 60W Si 25%$N_2$ | 44.87% | 28.74% | 26.39% |

In pioneer work done in this field, silicon content in the TiSiN film exhibiting highest hardness ranges from 7% to 12% [1]. In this study, a general trend of increasing hardness with increasing power on silicon target was observed at high silicon content and 20% $N_2$ composition. The film yielded highest hardness was the film deposited with 60W power on the Si target. Then $N_2$ was increased to 25% of the total gas mixture to assess the effects of $N_2$ composition on coating properties. A slight increase in hardness was observed.

Figure 4.20, 4.21, 4.6, and 4.22 represent the cross section of wear track of 50 W, 55 W, 60 W Si power, and 60 W Si power with 25% $N_2$, respectively. The graphs were generated using origin software. The width of the wear track was obviously larger at lower power on Si target. Sample prepared using 60 W power on Si targets, regardless of the $N_2$ composition in the chamber, had shallower and flatter wear track, which was an indication of better tribological coating. Samples prepared using higher power on silicon target also have better wear resistance, since lower wear rates were observed. COF, width and depth of the wear track,

hardness and wear rates are listed in Table 4.4.

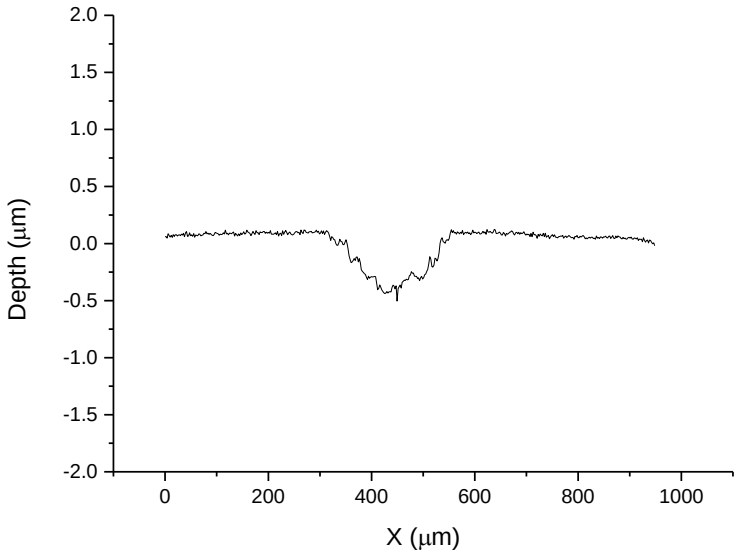


Figure 4.20. Cross section of wear track of TiSiN 100 V bias, 50 W Si power plotted in Origin

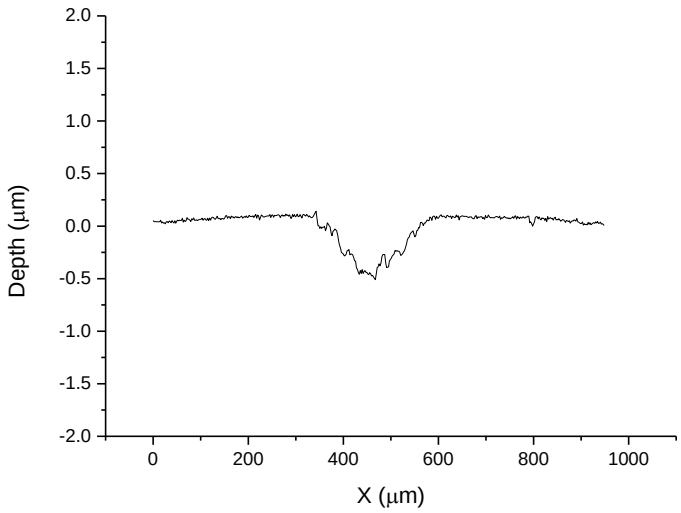


Figure 4.21. Cross section of wear track of TiSiN 100 V bias, 55 W Si power plotted in Origin

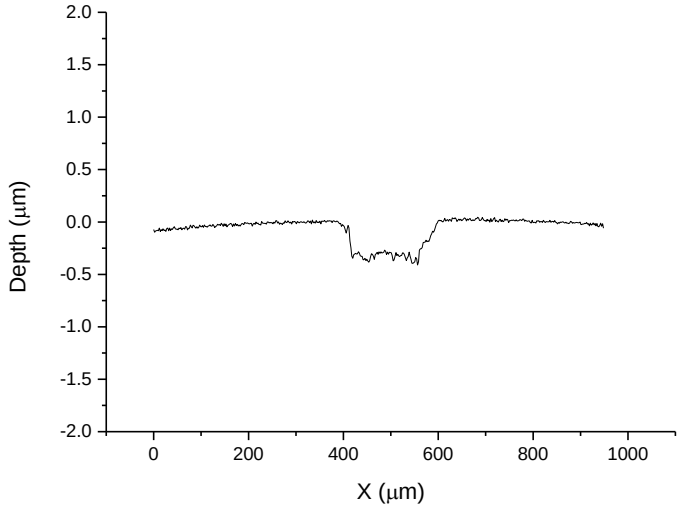


Figure 4.22. Cross section of wear track of TiSiN 100 V bias, 60 W Si power, 25% $N_2$ plotted in Origin

Figure 4.23, Figure 4.24, Figure 4.10, and Figure 4.25 are 2-D and 3-D images of TiSiN thin film with 50 W power, 55 W power, 60 W power applied to Si target and 60 W power with 25%$N_2$, respectively,. The results were obtained using optical profilometer. As discussed in section 4.1, spikes have been observed in the wear track of hard films. Figure 4.24 clearly shows the presence of debris in the track. This observation supports the theory that three body wear system occurred during wear test of hard thin film.

Table 4.4. Tribological experiment conditions and results of TiSiN varying Silicon power and Nitrogen composition

| Silicon Power (Bias 100V) | Wear Track Radius (mm) | Wear Track Width (μm) | Wear Track Depth (μm) | Wear Rate ($mm^3$/N*m) | COF | Hardness (GPa) [50] |
|---|---|---|---|---|---|---|
| 50W 20%N | 15 | 239 | 0.537 | 1.58E-05 | 1.15 | 34.5 |
| 55W 20%N | 17 | 231 | 0.593 | 1.86E-05 | 1.13 | 35.8 |
| 60W 20%N | 6 | 180 | 0.324 | 7.90E-06 | 1.10 | 37.1 |
| 60W 25%N | 9.5 | 181 | 0.423 | 9.76E-06 | 1.03 | 37.9 |

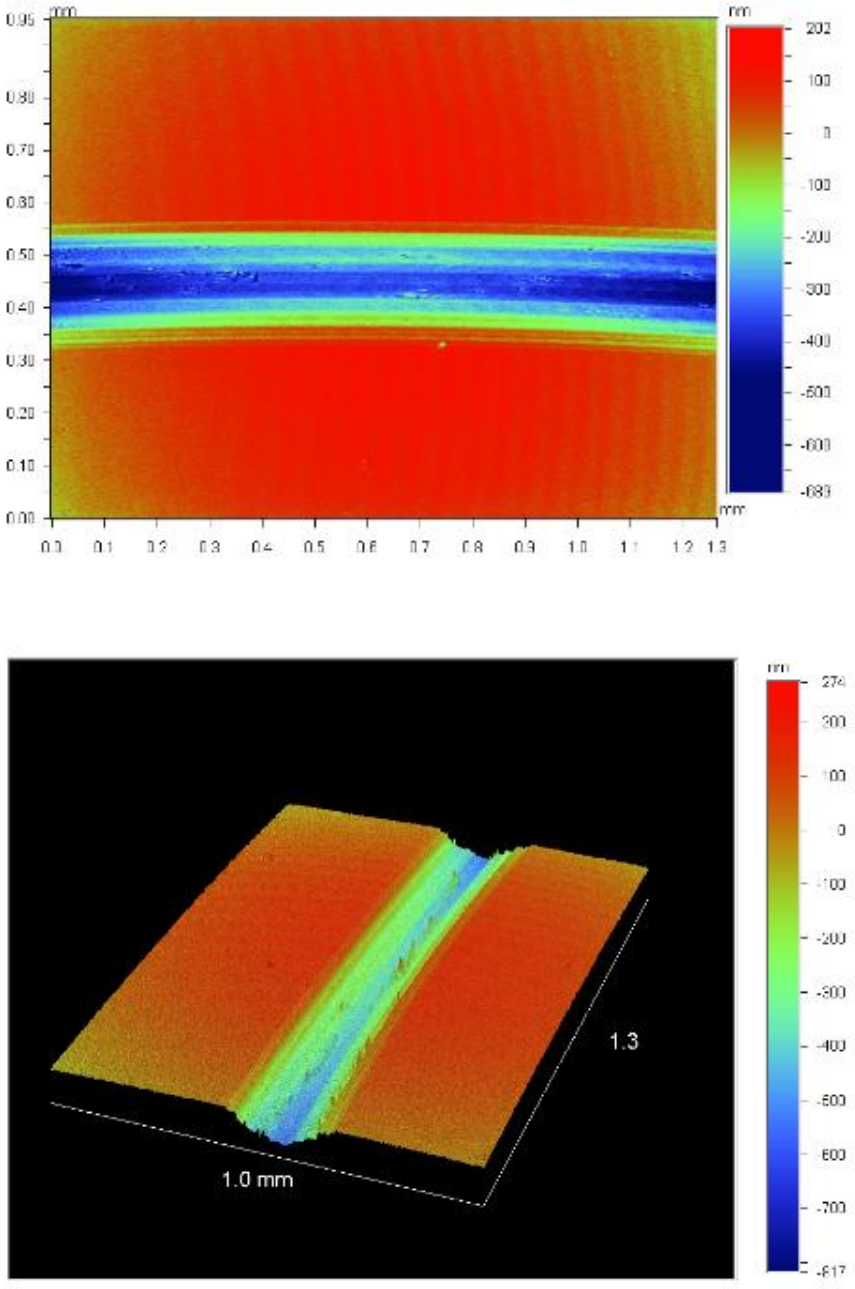


Figure 4.23. 2-D and 3-D image of wear track of TiSiN, 50 W Si power

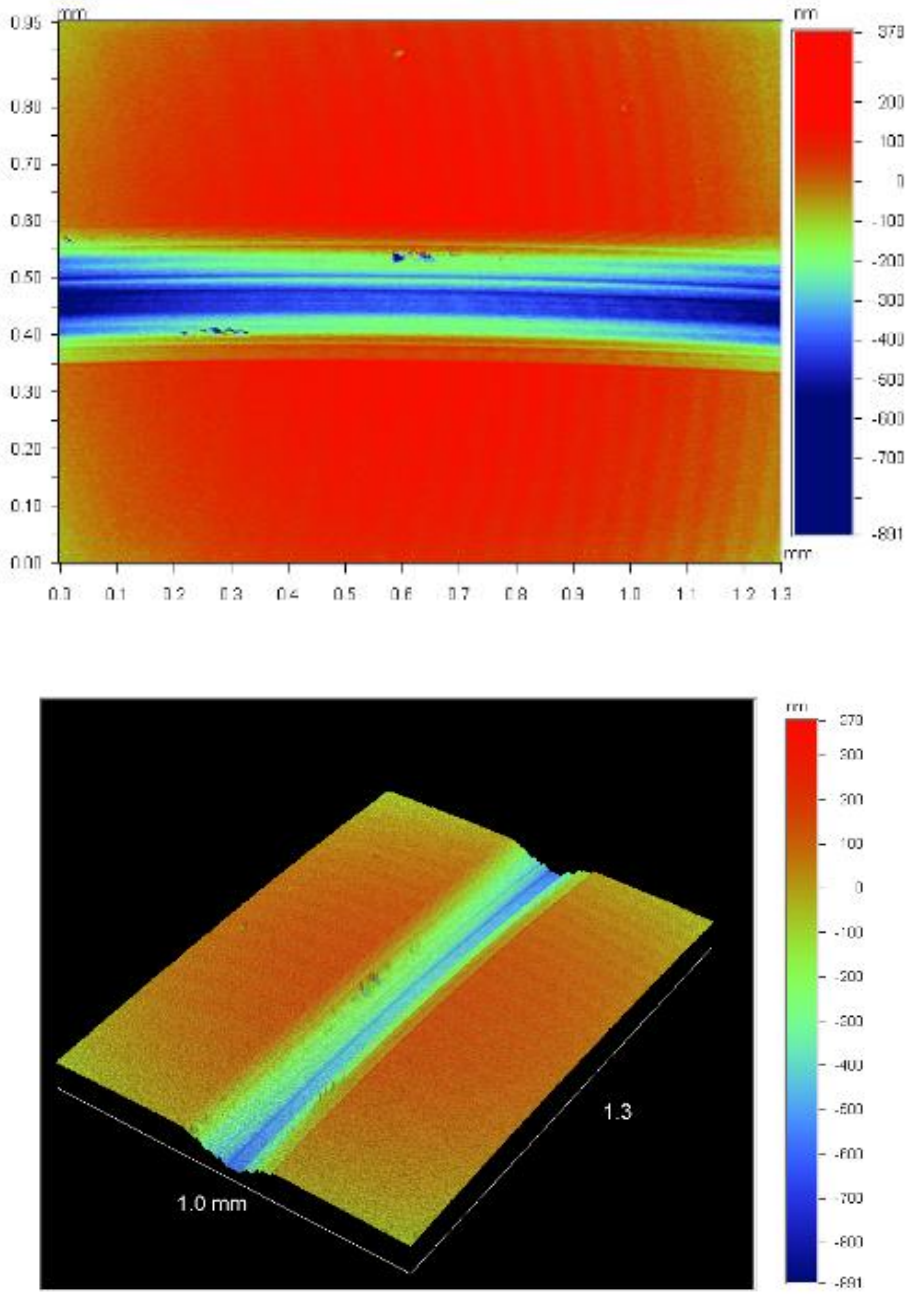


Figure 4.24. 2-D and 3-D image of wear track of TiSiN, 55 W Si power

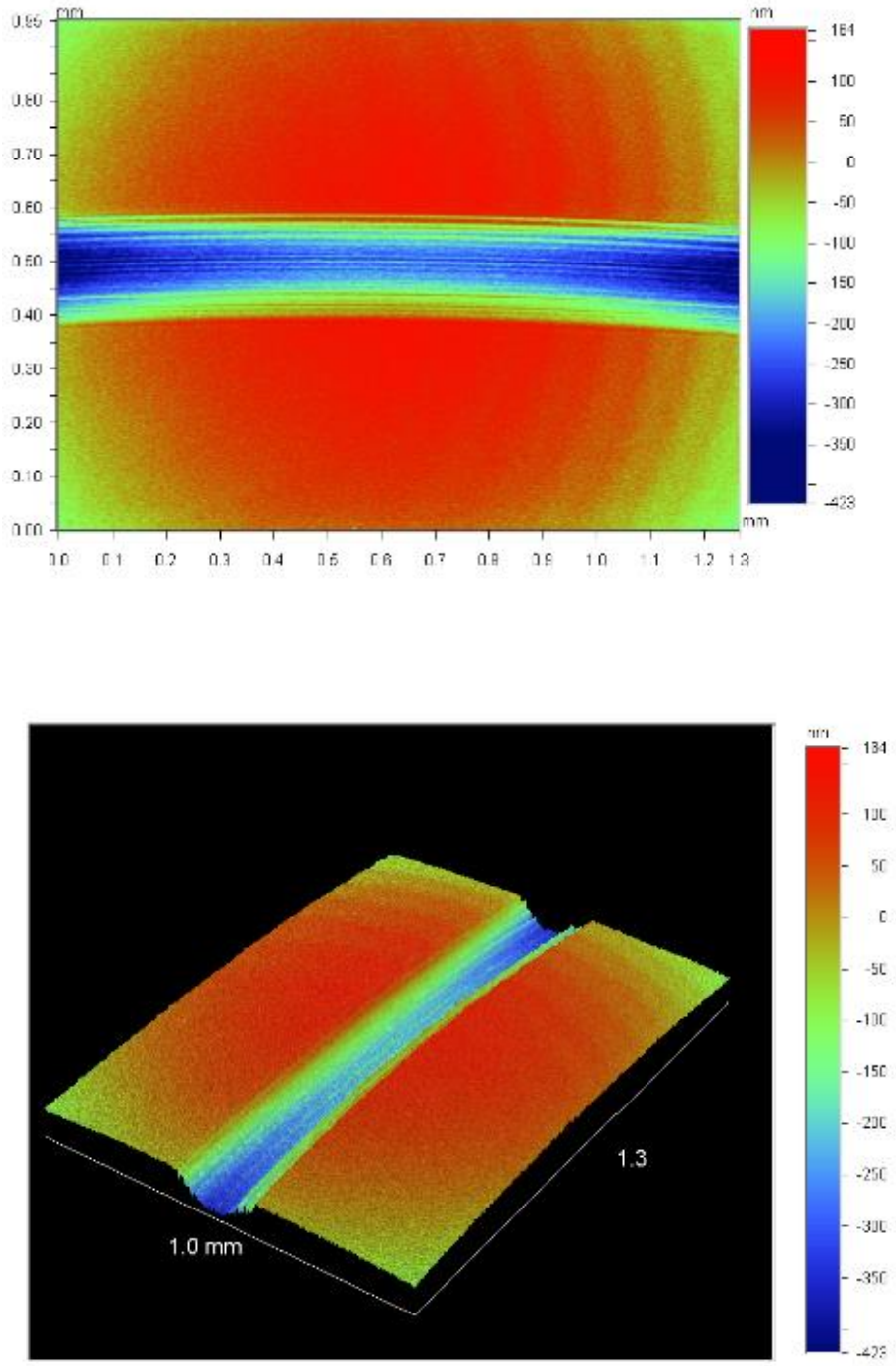


Figure 4.25. 2-D and 3-D wear track of TiSiN 60 W Si power, 25%$N_2$ at 3RPM

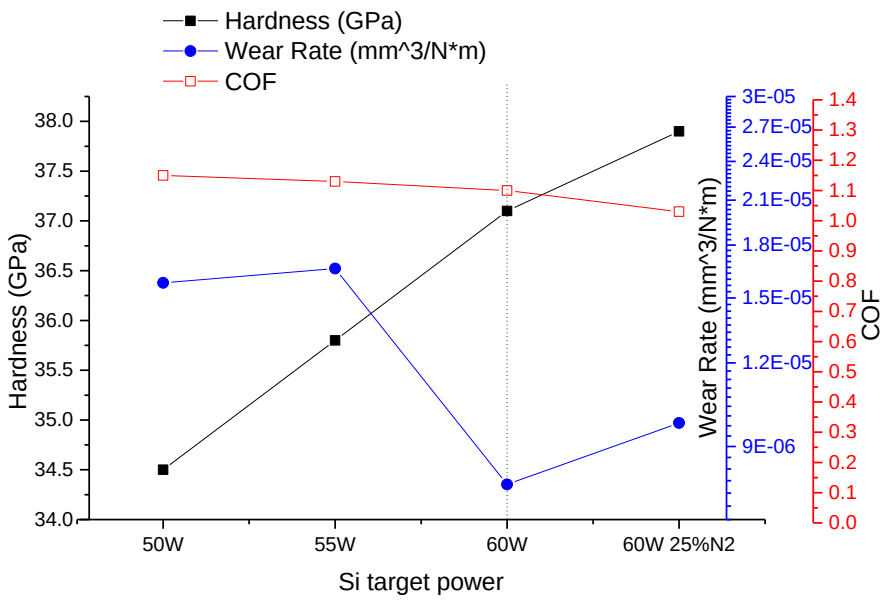


Figure 4.26. Effect of power Si target and $N_2$ content on mechanical properties of TiSiN

In this experimental section, we found that as the power applied on the Si target increases, a higher hardness of the film was achieved. The hardness of TiSiN enhanced again with a higher ratio of $N_2$ gas in the $N_2$/Ar mixture. The relationship of Si target power and nitrogen content with the wear rate, COF and hardness are shown in Figure 4.26

## 4.3 Effect of Substrate Rotation on Mechanical Properties of TiSiN

From 4.1 and 4.2, we determined that the condition to deposit TiSiN with higher hardness and better wear resistivity was to apply 100 V bias on the substrate, a power of 60 W utilized on Si target and a chamber gas ratio of $N_2$: Ar

at 1:3. In this experimental section, we will continue to explore the optimal condition of producing TiSiN with higher hardness and higher wear resistance in varying rotation speed of the substrate.

The substrate holder was rotated during the deposition at a certain speed to ensure the uniformity of the coating. Because two target materials were used simultaneously at different angles, left side of the chamber where the Si target was loaded would be Si rich, and front portion of the chamber would be Ti rich since the Ti target was loaded there. By rotating the substrate holder at a constant speed, a certain degree of uniformity could be achieved. Samples tested in previous experimental sections were all synthesized with 3 RPM rotation speed of the substrate holder. 3 RPM along with other two speeds, 1 RPM and 6 RPM, were used in this study to assess the effect of rotation speed on mechanical properties of TiSiN.

Wear test was performed using conditions similar to the conditions used in last experimental section. Counter materials used in all three tests were alumina ball with 1/4 inch radius. The linear speed used was 10 cm/s, and the load applied was 1 newton. The radius of the track and the results of the tribological test were recorded in table 4.5.

Figure 4.27, figure 4.19 and figure 4.28 represent the COFs of the samples with 1 RPM, 3 RPM, and 6 RPM, respectively. All three samples exhibited high coefficient of friction. As discussed in studies, these observations are assumed to

be caused by excessive amount of Si being present in the coating.

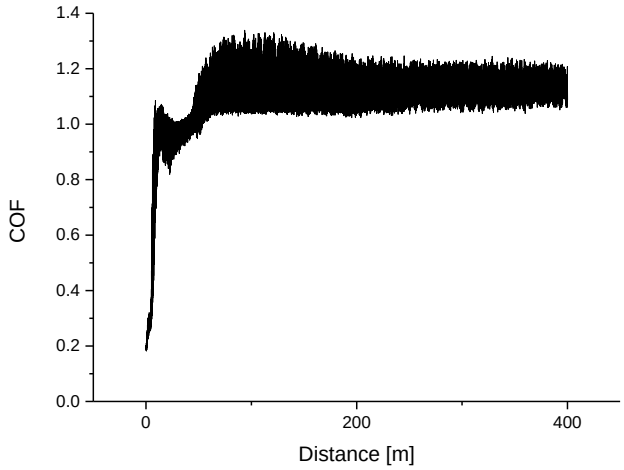


Figure 4.27. Wear test result of TiSiN 100 V bias, 60 W Si power, 25% $N_2$ at 1RPM

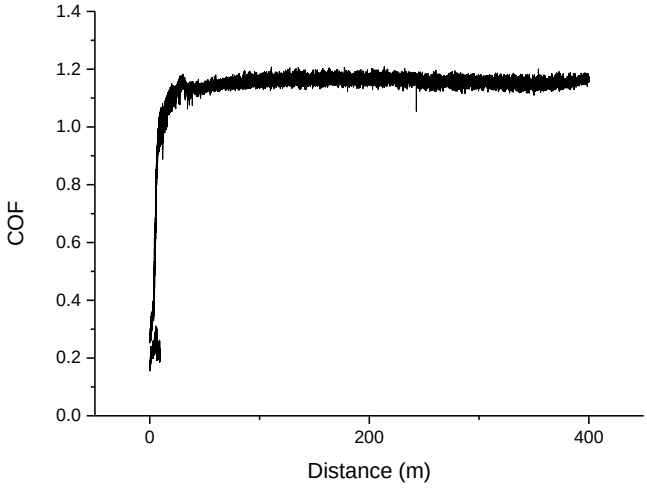


Figure 4.28. Wear Test Result of TiSiN 100 V bias, 60 W Si power, 25% $N_2$ at 6 RPM

Table 4.5. Tribological experiment conditions and results of TiSiN varying rotation speed of the substrate holder

| Sample | Wear Track Radius (mm) | Wear Track Width (μm) | Wear Track Depth (μm) | Wear Rate ($mm^3$/N*m) | COF | Hardness (GPa) [50] |
|---|---|---|---|---|---|---|
| 1 RPM | 15 | 207 | 0.357 | 9.83E-06 | 1.15 | 35.1 |
| 3RPM | 9.5 | 181 | 0.423 | 9.76E-06 | 1.03 | 37.9 |
| 6RPM | 19 | 172 | 0.404 | 9.55E-06 | 1.07 | 38.9 |

As shown in Table 4.5, increase of hardness was observed as the rotation speed was faster. The sample deposited at 6 RPM was the hardest sample out of all the samples tested in this study.

Shown in Figure 4.29, Figure 4.22, and Figure 4.30 are cross sections of the wear track of TiSiN deposited with variable rotation speed at 1 RPM, 3 RPM, and 6 RPM respectively. There were no significantly different wear rates for all three samples. Width of the wear track, on the other hand, decreased as the rotation speed increased, which may indicate better wear behavior at higher rotation speed. However, this is not conclusive because the reduction in width may also be the result of larger wear radius.

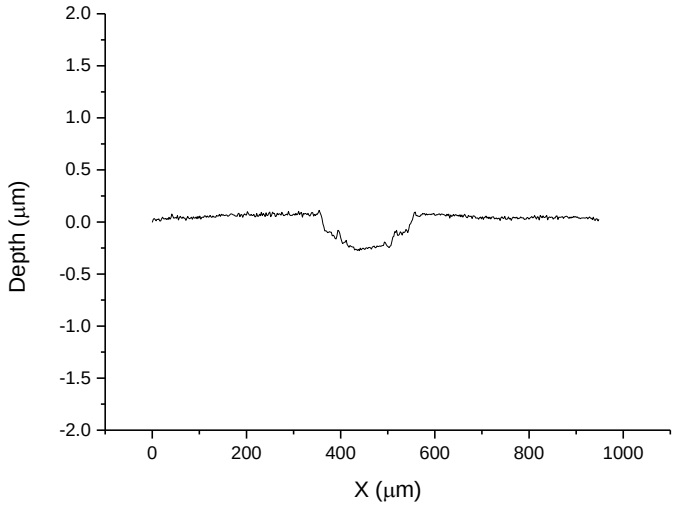


Figure 4.29. Cross section of wear track of TiSiN 1 RPM, 60 W Si, 100 V Bias, and 25% $N_2$

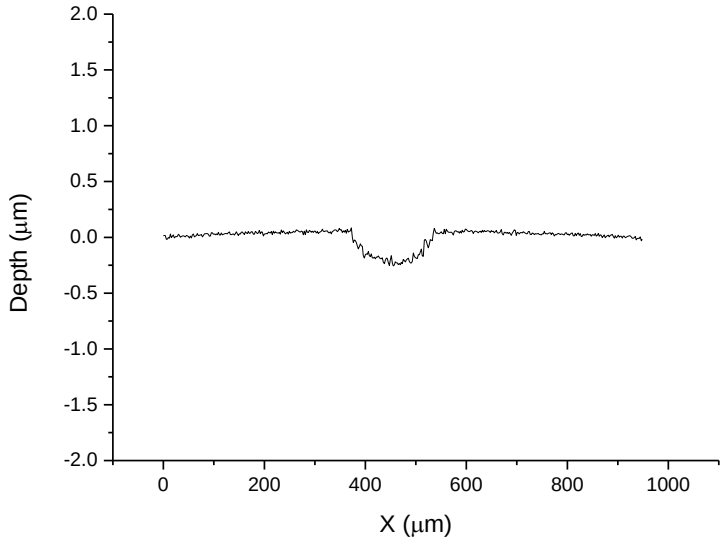


Figure 4.30. Cross section of wear track of TiSiN 6 RPM, 60 W Si, 100 V Bias, 25%$N_2$

Debris was present in the tracks again after the wear test. As discussed in previous experimental sections, the presence of debris may suggests a three-body wear system where not only the counter material and TiSiN were wearing each other, but the alumina debris was also partaking in the wearing process and causing an increase in both coefficient and wear rate. Presented in Figure 4.31, figure 4.25, and figure 4.32 are the images of the wear track of TiSiN coating with varying rotation speed of the substrate holder at 1 RPM, 3 RPM, and 6 RPM, respectively.

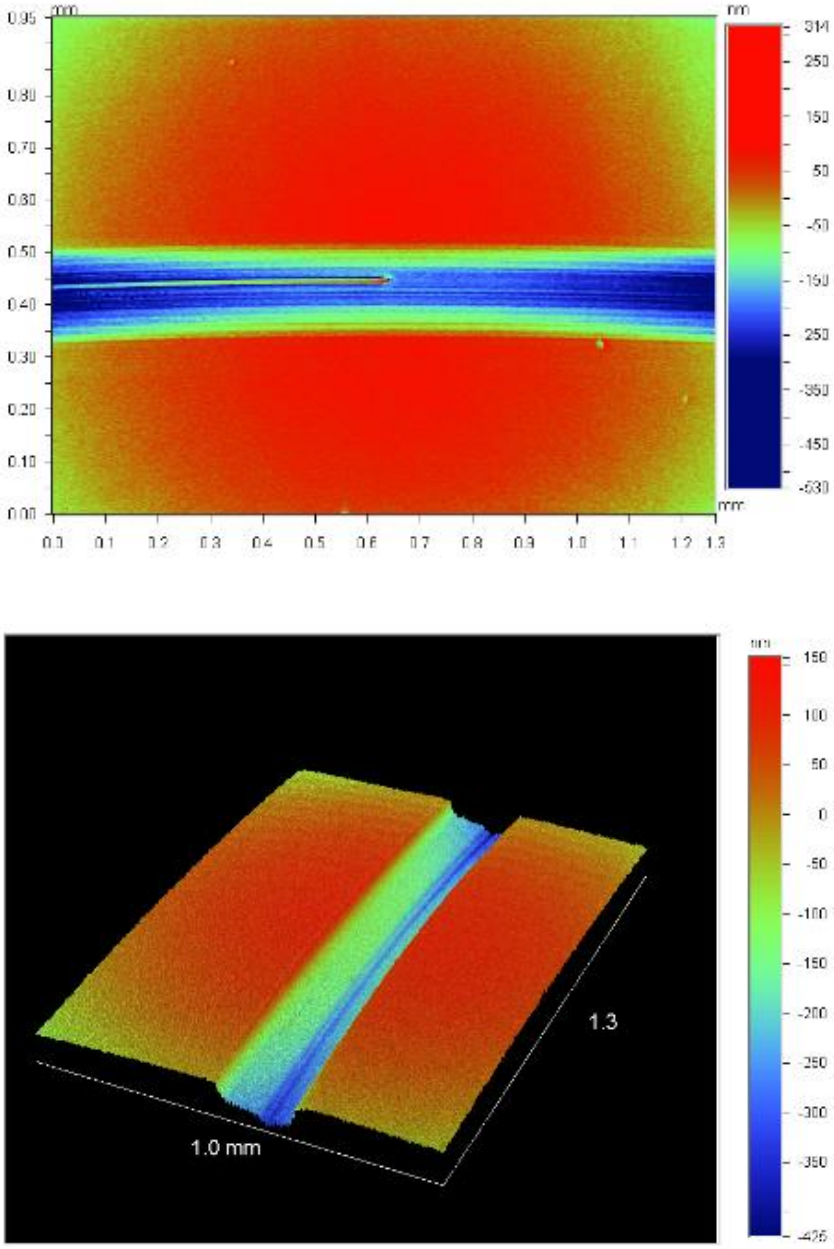


Figure 4.31. 2-D and 3D wear track image of TiSiN, 1 RPM

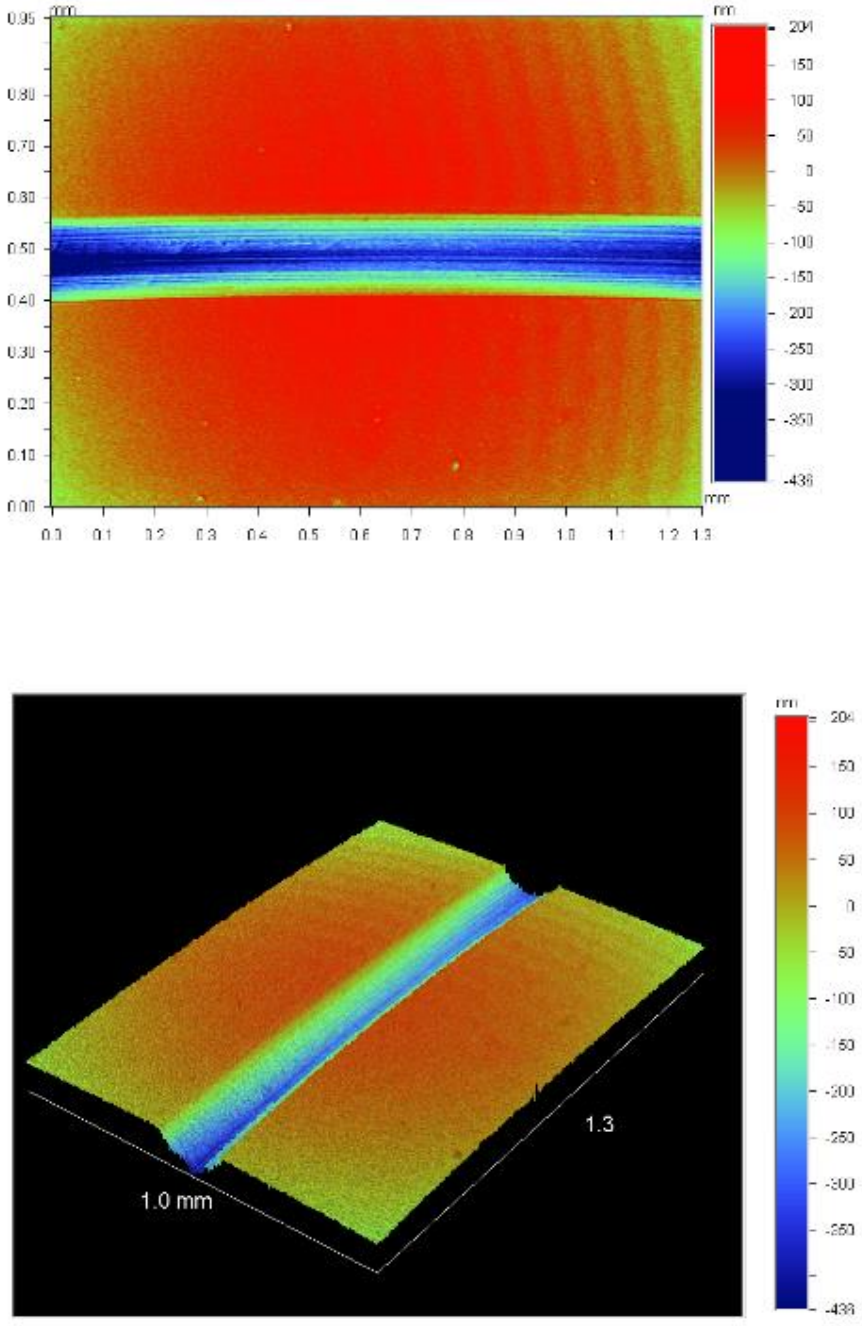


Figure 4.32. 2-D and 3D image of TiSiN, 6 RPM

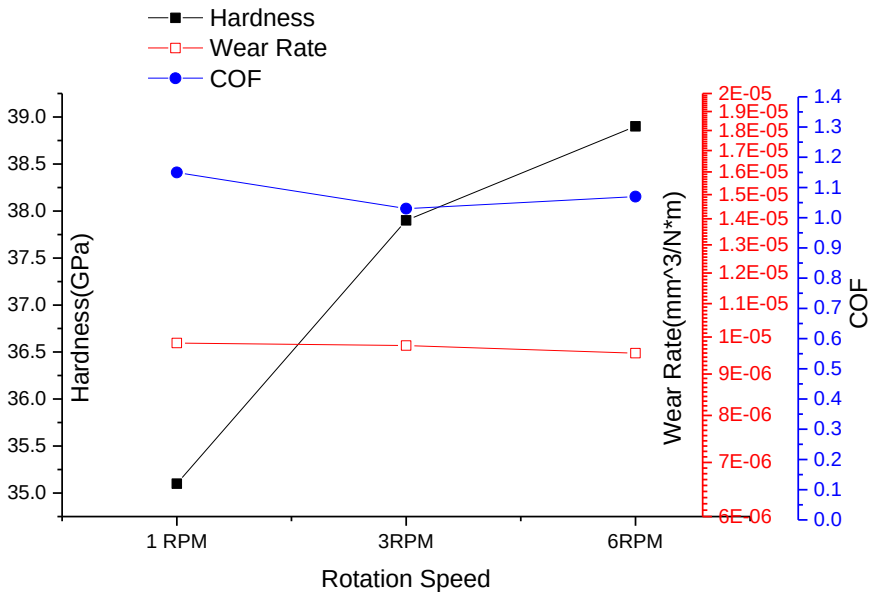


Figure 4.33. Effect of rotation speeds of substrate on mechanical properties of TiSiN

Figure 4.33 summarized the relationship of rotation speed with the hardness of the coatings, the wear rate, and the coefficient of friction. Hardness increased as the rotation speed increased. However, COF was high for all three samples and no significant changes in wear rate were observed. Further study with more rotation speeds may be required to determine an optimal rotation speed to produce TiSiN coating with highest hardness and wear resistance.

# Chapter 5

# CONCLUSION

TiSiN would exhibit a variety of mechanical properties depending on the deposition techniques and synthesis conditions. TiSiN films were deposited by Jessica Mooney, former graduate student at UT Arlington, using reactive PVD magnetron sputtering system. In this study, the effects of deposition parameters such as substrate bias, silicon power, $N_2$ to Ar ratio, and rotation speed of target to the mechanical properties of TiSiN thin film coating were determined.

Four different series of TiSiN films were produced. For all four series, power applied to Ti target was constant at 150 W, working pressure was 5 mTorr, and temperature of the substrate was 550 $^{\circ}$C.

First series of TiSiN films were deposited with 100V, 200V, 300V, and 500V bias applied to the substrate. Power applied to the Si target for the sample prepared at 100 V bias was 60 W. Power applied to the Si target for the other three samples prepared at 200 V, 300 V, and 500 V was 65 W. $N_2$ to Ar ratio was set at 1 to 4. It was found that COFs were high (>1) for all samples, and increasing substrate bias will lead to decrease in hardness and increase in wear rate. It was assumed that the high COFs were caused by the excessive Si content in the films. Sample synthesized with 100 V bias attained the highest hardness of 37.1 GPa. This sample also performed the best in tribological wear test and had lowest wear

rate, smallest wear track width, and more uniform wear track than the other three samples.

Based on the results for the first series, 100 V bias was selected as a constant parameter for the study of the second series. Three different Si power settings, 50 W, 55 W, 60 W were applied. $N_2$ to Ar ratio was set at 1 to 4. High COFs of greater than 1.0 were observed in all samples. As discussed earlier, this may be caused by the high Si content in the coatings. Additionally, white debris from the counter material (alumina) in the wear test was present in the wear tracks. This suggested a three body wear was introduced in the wear test, which may contribute to the high COFs. Si power setting at 60 W produced TiSiN film with the highest hardness of 37.1 GPa. Lower wear rate and better wear behavior were also observed in this sample. Another sample was deposited under the same conditions that produced the sample with hardness of 37.1 GPa except nitrogen gas to argon gas ratio in the chamber was increased to 1:3 from 1:4. The hardness increased slightly to 37.9 GPa. Wear rate and COFs stayed in the same range.

To further understand the effect of deposition conditions on mechanical properties of the TiSiN. The final batch of TiSiN films were deposited using different rotation speeds of the substrate (1 RPM, 3 RPM, and 6 RPM). Other synthesis conditions were set based on previous tests. 100 V bias was applied to the substrate, 60 W Si power was used, and $N_2$ to Ar ratio was set at 1:3. The results suggested that the rotation speed has no significant impact on COFs and

wear rates. Increase in hardness was observed as faster substrate rotation was utilized. Decrease in width of the wear track at high rotation speed may suggest a better wear behavior.

Scientists suggested that the maximum strength of TiSiN would be achieved at Si content of 8% to 12%. XPS results of the samples tested in this study showed that excessive amount of silicon (20% to 30%) were present in the film. Future work would involve lowering of Si content by using different deposition conditions.

References


1. Veprek, S. *Recent Research for new superhard materials: Go nano!*. Journal of Vacuum Science & Technology A, 31(5), (2013) 1-33.
2. Veprek, S. *The search for novel, superhard materials.* Journal of Vacuum Science & Technology A, 17(5), (1999) 2401-2420.
3. Musil, J., Vlcek J., and Zeman P. *Hard amorphous nanocomposite coatings with oxidation resistance above 1000℃.* Advances in Applied Ceramics, 107(3), (2008) 148-154.
4. Li, S. Z., Shi, Y., and Peng, H. R. *Ti-Si-N films prepared by plasma-enhanced chemical vapor deposition*. Plasma Chemistry and Plasma Process, 12(3), (1992) 287-297.
5. Veprek-Heijman, M. G. J., Veprek R. G., Argon, A. S., Parks, D. M., Veprek, S. *Non-linear finite element constitutive modeling of indentation into super- and ultrahard materials: The plastic deformation of the diamond tip and the ratio of hardness to tensile yield strength of super- and ultrahard nanocomposites*. Surface & Coatings Technology, 203(22), (2009) 3385-3391.
6. Veprek, S., Zhang, R. F., Veprek-Heijman, M. G. J., Sheng, S. H. and Argon, A. S. *Superhard nanocomposites: Origin of hardness enhancement,*

*properties and applications.* Surface & Coatings Technology, 204(12-13), (2010) 1898-1906.

7. Veprek, S., Zhang, R. F., Veprek-Heijman, M. G. J., Sheng, S. H. and Argon, A. S. *Search for Ultrahard Materials and Recent Progress in the Understanding of Hardness Enhancement and Properties of Nanocomposites.* Nanostructured Materials, Thin Films and Hard Coatings for Advanced Applications, 159, (2010) 1-10.
8. Veprek, S., Veprek-Heijman, M. G. J., and Zhang, R. F. *Chemistry, physics and fracture mechanics in search for superhard materials, and the origin of superhardness in nc-TiN/a-Si3N4 and related nanocomposites.* Journal of Physics and Chemistry of Solids, 68(5-6), (2007) 1161-1168.
9. Veprek, S. and Veprek-Heijman, M. G. J. *The formation and role of interfaces in superhard nc-MenN/a-Si3N4 nanocomposites.* Surface & Coatings Technology, 201(13), (2007) 6064-6070.
10. Prochazka, J., Karvankova, P., Veprek-Heijman, M. G. J. and Veprek, S. *Conditions required for achieving superhardness of >= 45 GPa in nc-TiN/a-Si3N4 nanocomposites.* Materials Science and Engineering a-Structural Materials Properties Microstructure and Processing, 384(1-2), (2004) 102-116.
11. Veprek, S., Niederhofer, A., Moto, K. Nesladek, P., Mannling, H. and Bolom T. *Nanocomposites nc-TiN/a-$Si_3N_4$/a- and nc-$TiSi_2$ with hardness*

*exceeding 100 GPa and high fracture toughness.* Materials Research Society, Symposium Proceedings, 581, (2000) 321-326.

12. Veprek, S. Weidmann, J. and Glatz, F. *Plasma chemical vapor deposition and properties of hard $C_3N_4$ thin films.* Journal of Vacuum Science & Technology A, 13, (1995) 2914-2919.
13. Chung, H. Y., Yang, J. M., Tolbert, S. H. and Kaner, R. B. *Anisotropic mechanical properties of ultra-incompressible, hard osmium diboride.* Journal of Materials Research, 23(6), (2008) 1797-1801.
14. Zhang, R. F., Legut, D., Niewa, R., Argon, A. S., and Veprek S. *Shear-induced structural transformation and plasticity in ultraincompressible ReB2 limit its hardness*. Physical Review B, 82(10), (2010) 1-7.
15. Chung, H. Y., Weinberger, M. B., Levine, J. B., Kavner, A., Yang, J. M., Tolbert, S. H., and Kaner, R. B. *Synthesis of Ultra-Incompressible Superhard Rhenium Diboride at Ambient Pressure.* Science, 316(5823), (2007) 436-439.
16. Veprek, S. Zhang, R. F., and Argon, A. S. *Mechanical properties and hardness of boron and boron-rich solids.* Journal of Superhard Materials, 33(6), (2011) 409-420.
17. Koehler, J. S. *Attempt to Design a Strong Solid.* Physical Review B, 2(2), (1970) 547-551.

18. Barnett, S. and Madan, A. *Superhard superlattice*. Physicals World, 11, (1998) 45-48.

19. Francombe, M. H. and Vossen, J. L. *Mechanic and Dielectric Properties*. 1993, Boston, MA: Academic Press.

20. McClintock, F. A. and Argon, A. S. *Mechanical Behavior of Materials*. 1966, Boston, MA: Addison-Wesley.

21. Hertzberg, R. W. *Deformation and Fracture Mechanics of Engineering Materials*. 1989, Hoboken, NJ: John Wiley & Sons.

22. Kelly, A., Macmillan, N. H. *Strong Solid*. 1986, Oxford, U.K.: Clarendon Press.

23. Carsley, J. E, Ning, J. Milligan, W. W., Hackney, S. A. and Aifantis, E. C. *A simple, mixture-based model for the grain size dependence of strength in nanophase metal*, Nanostructured Materials, 5(4), (1995) 441-448.

24. Zhang, S. *Nanostructured Thin Films and Coatings: Mechanical Properties*. 2010, New York, NY: Taylor and Francis Group, LLC.

25. Karvankova, P., Mannling, H., Eggs, C. and Veprek, S. *Thermal stability of ZrN–Ni and CrN–Ni superhard nanocomposite coatings*. Surface and Coatings Technology, 146, (2001) 280-285.

26. Koch, C. C., Ovidko, I. A., Seal, S., and Veprek, S. *Structural Nanocrystalline Materials, Fundamentals, and Applications*. 2007, Cambridge, UK: Cambridge University Press.

27. Koch, C. C., Scattergood, R. O., Saber, M., and Kotan, H. *High temperature stabilization of nanocrystalline grain size: Thermodynamic versus kinetic strategies*. Journal of Materials Research, 28(13), (2013) 1785-1791.

28. Hauert, R. and Patscheider, J. *From alloying to nanocomposites-Improved performance of hard coatings.* Advanced Engineering Materials, 2(5), (2000) 247-259.

29. Zhang, R.F. and Veprek, S. *Metastable phases and spinodal decomposition in Ti(1-x)Al(x)N system studied by ab initio and thermodynamic modeling, a comparison with the TiN-Si(3)N(4) system.* Materials Science and Engineering A-Structural Materials Properties Microstructure and Processing, 448(1-2), (2007) 111-119.

30. Zeman, P., Cerstvy, R., Mayrhofer, P. H., Mitterer, C. and Musil, J. *Structure and properties of hard and superhard Zr-Cu-N nanocomposite coatings.* Materials Science and Engineering A-Structural Materials Properties Microstructure and Processing, 289(1-2), (2000) 189-197.

31. Veprek, S., Meng, W. J., Kumar, A., Chung, Y. W., Doll, G. L. and Cheng, Y. T. *Different mechanisms leading to superhard coatings: Stable nanocomposites and high biaxial compressive stress*. MRS Proceedings, 697, (2001) 27-32.

32. Musil, J., Hruby, H., Zeman, P., Zeman, H., Cerstvy, R., Mayrhofer, P. H.

and Mitterer, C. *Hard and superhard nanocomposite Al-Cu-N films prepared by magnetron sputtering*. Surface & Coatings Technology, 142, (2001) 603-609.

33. Carvalho, S., Ribeiro, E., Rebouta, L., Pacaud, J., Goudeau, Ph., Renault, P. O. and Riviere, J. P. *PVD grown (Ti,Si,Al)N nanocomposite coatings and (Ti,Al)N/(Ti,Si)N multilayers: structural and mechanical properties.* Surface & Coatings Technology, 172(2-3), (2003) 109-116.
34. Prilliman, S. G., Clark, S. M., Alivisatos, A. P., Karvankova, P. and Veprek, S. *Strain and deformation in ultra-hard nanocomposites nc-TiN/a-BN under hydrostatic pressure.* Materials Science and Engineering A-Structural Materials Properties Microstructure and Processing, 437(2), (2006) 379-387.
35. Zhang, R.F. and Veprek, S. *Phase stabilities and spinodal decomposition in the Cr1-xAlxN system studied by ab initio LDA and thermodynamic modeling: Comparison with the Ti1-xAlxN and TiN/Si3N4 systems.* Acta Materialia, 55(14), (2007) 4615-4624.
36. Sheng, S.H., Zhang, R. F. and Veprek, S. *Study of spinodal decomposition and formation of nc-Al2O3/ZrO2 nanocomposites by combined ab initio density functional theory and thermodynamic modeling.* Acta Materialia, 59(9), (2011) 3498-3509.
37. Ivashchenko, V.I., Veprek, S., Turchi, P. E. A. and Shevchenko, V. I.

*First-principles study of TiN/SiC/TiN interfaces in superhard nanocomposites*. Physical Review B, 86, (2012) 1-8.

38. Cheng, Y. H., Browne, T. and Heckerman, B. *Nanocomposite TiSiN coatings deposited by large area filtered arc deposition*. Journal of Vacuum Science & Technology A, 27(1), (2009) 82-88.
39. Cheng, Y.H., Browne, T., Heckerman, B., Jiang, J. C., Meletis, E. I., Bowman, C. and Gorokhovsky, V . *Internal stresses in TiN/Ti multilayer coatings deposited by large area filtered arc deposition.* Journal of Applied Physics, 104, (2008) 1-7.
40. Veprek, S. *The origin of superhardness in TiN/$Si_3N_4$ nanocomposites: the role of the interfacial monolayer.* High Pressure Research, 26(2), (2006) 119-125.
41. Pogrebnjak, A.D., Shpak, A. P., Azarenkov, N. A. and Beresnev, V. M. *Structures and properties of hard and superhard nanocomposite coatings*. Physics-Uspekhi, 52(1), (2009) 29-54.
42. Schwaller, P., Haug, H. J., Michler, J. and Patscheider, J. *Nanocomposite hard coatings: Deposition issues and validation of their mechanical properties.* Advanced Engineering Materials, 7(5), (2005) 318-322.
43. Thornton, J.A. *Influence of Apparatus Geometry and Deposition Conditions on Structure and Topography of Thick Sputtered Coatings.* Journal of Vacuum Science & Technology, 11(4), (1974) 666-670.

44. Thornton, J.A. *High-Rate Thick-Film Growth.* Annual Review of Materials Science, 7, (1977) 239-260.

45. Veprek, S. and Reiprich, S. *A concept for the design of novel superhard coatings.* Thin Solid Films, 268(1-2), (1995) 64-71.

46. Veprek, S., Reiprich, S. and Li, S. H. *Superhard Nanocrystalline Composite-Materials - the Tin/Si3n4 System.* Applied Physics Letters, 66(20), (1995) 2640-2642.

47. Veprek, S. and Argon, A. S. *Towards the understanding of mechanical properties of super- and ultrahard nanocomposites.* Journal of Vacuum Science & Technology B, 20(2), (2002) 650-664.

48. Zhang, R.F. and Veprek, S. *On the spinodal nature of the phase segregation and formation of stable nanostructure in the Ti-Si-N system.* Materials Science and Engineering a-Structural Materials Properties Microstructure and Processing, 424(1-2), (2006) 128-137.

49. Zhang, R.F. and Veprek, S. *Phase stabilities of self-organized nc-TiN/a-Si(3)N(4) nanocomposites and of Ti(1-x)S(x)N(y) solid solutions studied by ab initio calculation and thermodynamic modeling.* Thin Solid Films, 516(8), (2008) 2264-2275.

50. Mooney, J. *The Effects of Microstructure on the Mechanical Properties of Hard Transition Metal Silicon Nitride Nanocomposite Coatings.* Dissertation, UT Arlington. 2013.

51. Veprek, S., Prochazka, J., Karvankova, P. and Veprek-Heijman, M. G. J. *Different approaches to superhard coatings and nanocomposites.* Thin Solid Films, 476(1), (2005) 1-29.

52. Chung, C.K. and Su, P. J. *Material characterization and nanohardness measurement of nanostructured Ta-Si-N film.* Surface & Coatings Technology, 188-189, (2004) 420-424.

53. Bunshah, R.F. *Handbook of deposition technologies for films and coatings: science, technology, and applications*. 1994, Park Ridge, NJ: Noyes Publications.

54. Veprek, S., Karvankova, P. and Veprek-Heijman, M. G. J. *Possible role of oxygen impurities in degradation of nc-TiN/a-Si3N4 nanocomposites.* Journal of Vacuum Science & Technology B, 23(6), (2005) L17-L21.

55. Tudora, I., Popescub, A., Ripeanua, R. G., Drumeanua, A. C., Braicc, V., Balaceanuc, M., Vladescuc, A., Braic, M. *Tribological behaviour of TiSiN/Ti and TiSiN/Cu multilayer coatings*. Journal of the Balkan Tribological Association, 15(2), (2009) 156-162.

56. Savaskan, T. and Bican O. *Effects of Silicon Content on the Microstructural features and mechanical and sliding wear properties of Zn–40Al–2Cu–(0–5)Si alloys.* Materials Science and Engineering A, 404(1-2), (2005) 259–269.

## Biographical Information

Suo Liu was born in Jianshi, P. R. China. Suo Liu obtained a Bachelor of Science in Biological and Agricultural Engineering at Texas A&M University in 2011. His undergraduate project was survey and design of natural channel. He worked as an assistant manager in T'Jin Chinese Restaurant after graduation from Texas A&M University.

In August of 2013, Suo Liu started his Master of Science education in Materials Science and Engineering Department at University of Texas at Arlington. He conducted his research under the guidance of Dr**.** E. I. Meletis in the Surface and Nano Engineering Laboratory. Suo Liu's research project focused on characterization of Titanium Silicon Nitride films deposited using reactive PVD magnetron sputtering.